Stratigraphic record of subduction initiation in the Permian metasedimentary succession of the El Paso Mountains, California

Jean L. Rains, Kathleen M. Marsaglia, and George C. Dunne
DEPARTMENT OF GEOLOGICAL SCIENCES, CALIFORNIA STATE UNIVERSITY–NORTHRIDGE, 18111 NORDHOFF STREET, NORTHRIDGE, CALIFORNIA 91330-8266, USA

ABSTRACT

Petrologic investigation of Permian metasedimentary rocks in the El Paso Mountains reveals a rock record interpreted to be consistent with the sedimentary pattern of the upper continental plate of a nascent subduction zone, based on geodynamic modeling and comparison with a Cenozoic example (Puysegur Ridge, New Zealand). Facies changes reveal a history of uplift (conglomerate), followed by subsidence (carbonate turbidite deposits) and deeper-water sedimentation (argillite, with portions deposited below the carbonate compensation depth [CCD]), and then gradual shallowing accompanied by the onset of nearby intermediate volcanism (volcaniclastic and bioclastic sediments) and construction of a volcanic edifice (andesitic lavas) in a shallow-marine environment. Comparison with Permian global sea-level curves indicates that initial uplift (relative sea-level fall) followed by deep subsidence (relative sea-level rise) are likely due to tectonic rather than eustatic effects. Shallowing during volcaniclastic sedimentation could have been due to both arc edifice building and global sea-level fall. Sandstone modal analysis suggests that the basin evolved from a tectonic setting involving compressive uplift to an arc basin setting. Geodynamic modeling implies the involvement of a transform/truncation fault in subduction initiation. Magmatic trends based on Permian paleogeography and timing suggest a limited nucleation of subduction in the El Paso Mountains followed by propagation southward. Furthermore, subduction initiation modeling suggests regional lithospheric flexure that may be reflected in coeval basins and uplift in the northern Mojave, Death Valley, and Inyo Mountains regions as well as in coeval facies changes on the western edge of the Colorado Plateau. Overall, the Permian section of the El Paso Mountains may be one of the few preserved Paleozoic sedimentary records of subduction inception along a continental margin.

LITHOSPHERE; v. 4; no. 6; p. 533–552 | Published online 3 April 2012 doi: 10.1130/L165.1

INTRODUCTION

Recent geodynamical modeling of subduction initiation suggests that this plate-tectonic process should produce distinct sedimentary records on the overriding plate margin depending on the manner of subduction initiation (cf. Marsaglia, 2012; for distinctions between "forced" or "induced" subduction initiation and "spontaneous" subduction initiation, see Gurnis et al., 2004; Stern, 2004; Nikolaeva et al., 2011). However, subsequent magmatism and deformation may obscure or remove this record (Sutherland et al., 2006; Gurnis et al., 2004; Stern, 2004; Hall et al., 2003). We know of no prior work specifically documenting the sedimentary fingerprint of this process in the rock record but have found a good candidate in the Lower Permian section of the El Paso Mountains, southern California. Building on the work of Carr et al. (1997), our more detailed petrologic study in combination with new geodynamic models for subduction inception allow us to interpret the Permian metasedimentary to volcanic succession in the El Paso Mountains as a product of induced subduction initiation. As such, this succession in the El Paso Mountains may be one of the first formally described and best-preserved examples of this tectonic transition.

Editor's note: This article is part of a special issue titled "Initiation and Termination of Subduction: Rock Record, Geodynamic Models, Modern Plate Boundaries," edited by John Shervais and John Wakabayashi. The full issue can be found at http://lithosphere.gsapubs.org/content/4/6.toc.

GEOLOGIC BACKGROUND

Regional Tectonic and Depositional Setting

During the Paleozoic, the Cordilleran margin of North America underwent a rearrangement of the margin trend and a tectonic transition from passive margin to active subduction. In the early Paleozoic (Cambrian to Devonian), the Cordilleran margin of North America was a passive margin with a NE-SW trend (Fig. 1), as evidenced by sedimentary patterns (Hamilton and Myers, 1966; Burchfiel and Davis, 1972) and the $^{87}Sr/^{86}Sr_i = 0.706$ line (Kistler and Peterman, 1973). By Triassic time, an active continental margin with subduction had been established along a reoriented NW-SE–trending margin (Walker, 1988; Dickinson, 2000; Stevens et al., 2005). However, many aspects of this passive-to-active transition remain poorly known, and, as a result, much debated in the literature (e.g., Snow, 1992; Dickinson, 2000; Stevens et al., 2005).

One approach to deciphering this tectonic transition is examination of the stratigraphy of sparse basin-fill remnants along the margin. These stratigraphic records, including those in the El Paso Mountains of southern California (Figs. 1, 2, and 3), were previously examined by Carr et al. (1984, 1997) and Martin and Walker (1995), and references therein.

As part of the transition, early Paleozoic passive-margin sedimentation was interrupted in Nevada and northern California by the Antler orogeny as oceanic rocks (the Roberts Mountains allochthon) were thrust over miogeoclinal rocks in latest Devonian to earliest Mississippian time (Dickinson, 2006). Assemblages of Antler-related rocks at Miller

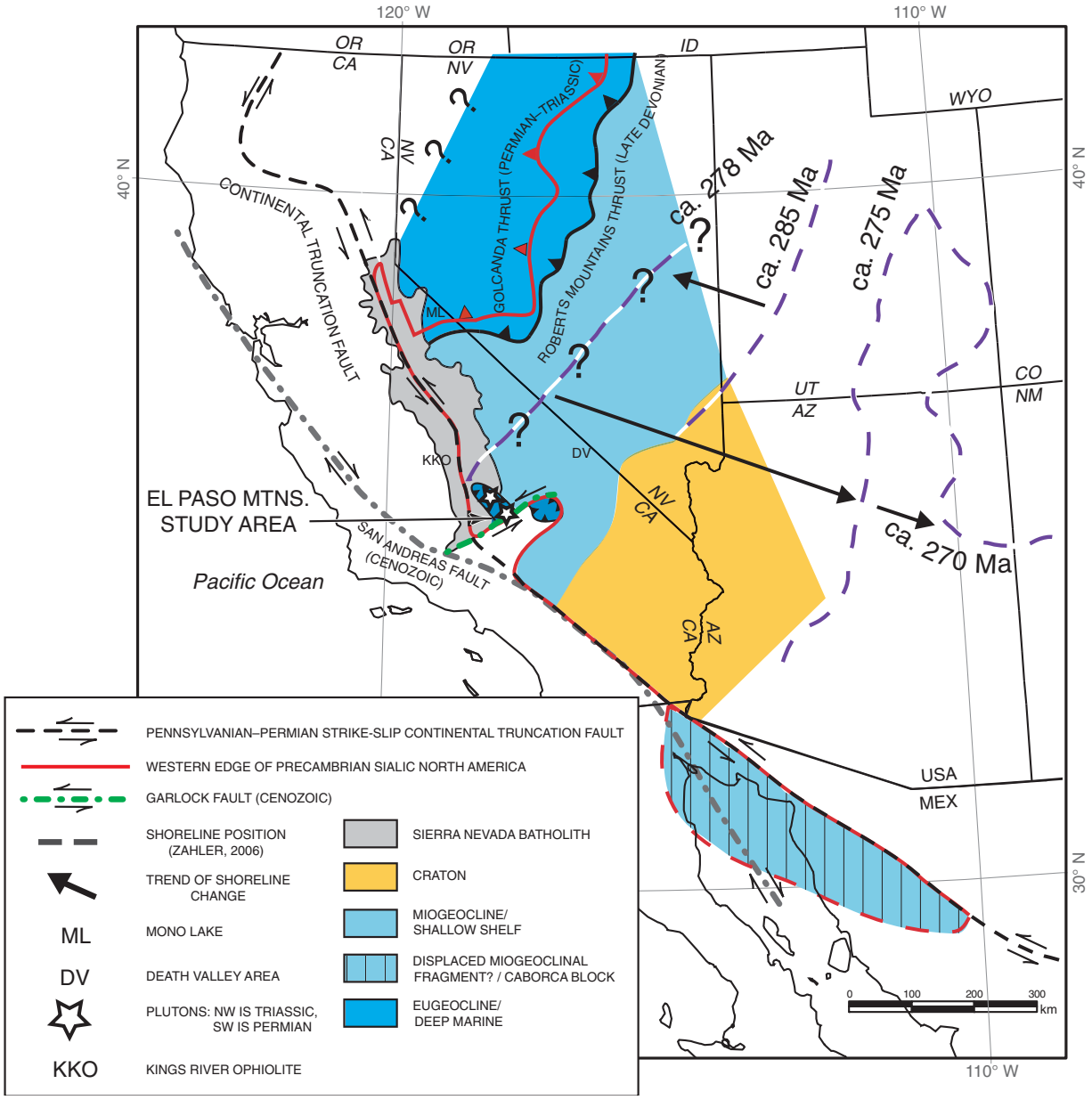

Figure 1. Regional tectonic map of southwestern North America, with the proposed Pennsylvanian–Permian continental truncation fault. On the regional map, early Paleozoic passive-margin facies belts (areas in color) all trend northeast, in contrast to the northwest trend of the Sierra Nevada Batholith and the proposed Pennsylvanian–Permian truncation line (eugeocline—ocean basin and continental rise, miogeocline—continental shelf and craton). The El Paso Mountains are interpreted by many authors (see text references) as part of a displaced terrane (El Paso terrane) of early Paleozoic continental-rise strata that was stranded during Pennsylvanian–Permian left-lateral continental truncation; the miogeoclinal (shelfal) Caborca block displacement is also linked to truncation. Stars indicate the location of El Paso terrane plutons: to the southeast, the Permian El Paso Mountains pluton; to the northwest, the early Triassic southern Sierra Nevada pluton. Thrust faults surrounding the terrane reflect west-vergent folding and thrusting in the latest Permian, likely linked to Permian subduction (Carr et al., 1997), and later eastward displacement onto continental substratum between ca. 240 Ma and 179 Ma (Miller et al., 1995). Movement on the Cenozoic left-lateral Garlock fault bisected the terrane. Locations of plutons are from Carr et al. (1997) and Dunne and Saleeby (1993). Figure is modified after Dickinson et al. (2000) and Stevens et al. (2005).

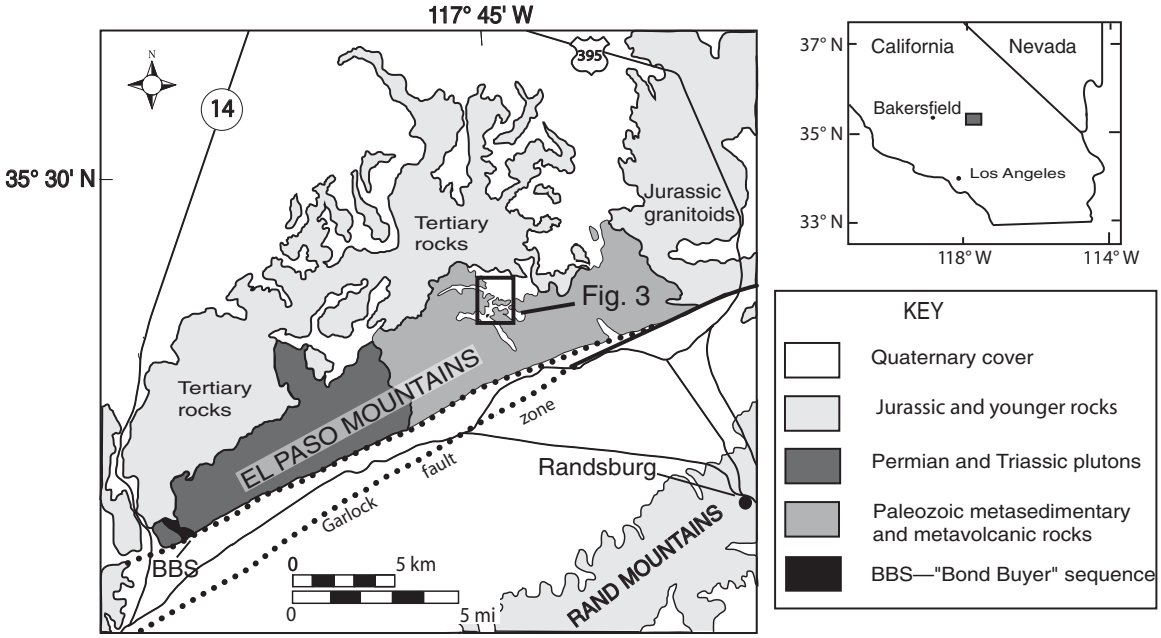

Figure 2. Location map of the El Paso Mountains study area northeast of Los Angeles, California, between California Highway 14 and U.S. Highway 395. The Bond Buyer sequence (BBS), which includes Lower Permian andesite, is located at the western end of the El Paso Mountains. Location map is modified after Carr et al. (1984).

Mountain in west-central Nevada belonging to the Roberts Mountains allochthon have been correlated with Lower and Middle Paleozoic rocks of the El Paso Mountains (Carr et al., 1984, 1997), and Upper Mississippian rocks of the El Paso Mountains have been correlated with Antler foreland basin deposits (Carr et al., 1984).

The Lower Paleozoic strata of the western El Paso Mountains (Carr et al., 1997; Stevens et al., 2005) are eugeoclinal rocks (deep-water facies) that appear to have originated as part of the passive-margin eugeoclinal belt that trends from northwestern Nevada into the central Sierra Nevada in California (Fig. 1), but are now juxtaposed against miogeoclinal rocks without intervening facies (Stevens et al., 2005). It is debated as to whether the Lower Paleozoic rocks of the El Paso Mountains were displaced southward from the Antler belt, and, if so, by what means (e.g., Carr et al., 1984; Snow, 1992; Dickinson, 2000; Stevens et al., 2005). Several authors have postulated displacement by a left-lateral transform fault as part of the reorientation of the continental margin (Carr et al., 1997, 1984; Dickinson, 2000; Stevens et al., 2005). The extension of the Antler belt to the latitude of the El Paso Mountains has also been suggested (Stone, 1984); however, no structural indications of the Antler orogeny have been observed at the present latitude of the El Paso Mountains (Carr et al., 1997). Dickinson (1981), among others, proposed that the original Proterozoic rifted margin was irregular, with miogeoclinal trends following a jagged continental margin; therefore, little or no modification of the margin was required prior to later subduction initiation. Stone (1984) similarly proposed that truncation, if it had occurred, was subparallel to an irregular margin. He interpreted the sediment belt from the Antler orogeny to be wide along the southwestern trend of the margin through Nevada and then narrow as it turned southeast in California.

The apparent southward displacement of the El Paso Mountains from about the latitude of Mono Lake (Stevens et al., 2005; Dickinson, 2006) and the apparent displacement of the Caborca block (miogeoclinal rocks similar to the Cordilleran sequence in Death Valley; Burchfiel and Davis, 1981) from their respective Lower Paleozoic facies belts (Stewart et al., 1984, 1990; Ketner, 1986; Ketner and Noll, 1987), along with other evidence (see previous references), have been interpreted as supporting continental margin rearrangement by left-lateral faulting (Fig. 1) (Burchfiel and Davis, 1972, 1975; Dickinson, 2000; Stevens et al., 2005). In this interpretation, outcrops of Antler-related rocks found in the El Paso Mountains, northwest Mojave Desert, and roof pendants in the Kern Plateau of the Sierra Nevada (Dunne and Suczek, 1991) (Fig. 1) were left behind in fault-bound slivers near the truncation fault as the main body of rock was moved into northern Mexico. The parts of this "El Paso terrane" are broadly arranged from west to east, from deepest facies (Kern Plateau) to the shallowest (El Paso Mountains), although individual displacements are uncertain (cf. Carr et al., 1997; Dunne and Suczek, 1991).

The rearrangement of the continental margin was associated with and followed by the initiation of subduction along the now NW- to SE-trending margin. Development of subduction and an associated magmatic arc is indicated by Late Permian through Late Triassic plutons stretched along a NW-SE–trending belt from west-central Nevada through California into what is now Sonora, Mexico (Miller et al., 1995; Barth et al., 1997; Stevens et al., 2005; Barth and Wooden, 2006; Arvisu et al., 2009). Throughout their geographic distribution, the ages of the plutons are mixed. There are fewer Late Permian and Early Triassic plutons, and more Middle and Late Triassic plutons (Stevens et al., 2005). The late Early Permian–age pluton in the El Paso Mountains is one of the few Permian plutons and the oldest in the southern half of California (Miller et al., 1995; Barth et al., 1997; Barth and Wooden, 2006) (Fig. 1).

The plutons also vary in terms of the nature of the lithosphere into which they were emplaced: Northern California Permian plutons were emplaced in intraplate oceanic crust (Dickinson, 2000), a Permian pluton in NW Sonora, Mexico, was emplaced into continental lithosphere (Arvisu et al., 2009), and the El Paso Mountains Permian pluton was emplaced into outer or "thinned" continental lithosphere (Barth and Wooden, 2006;

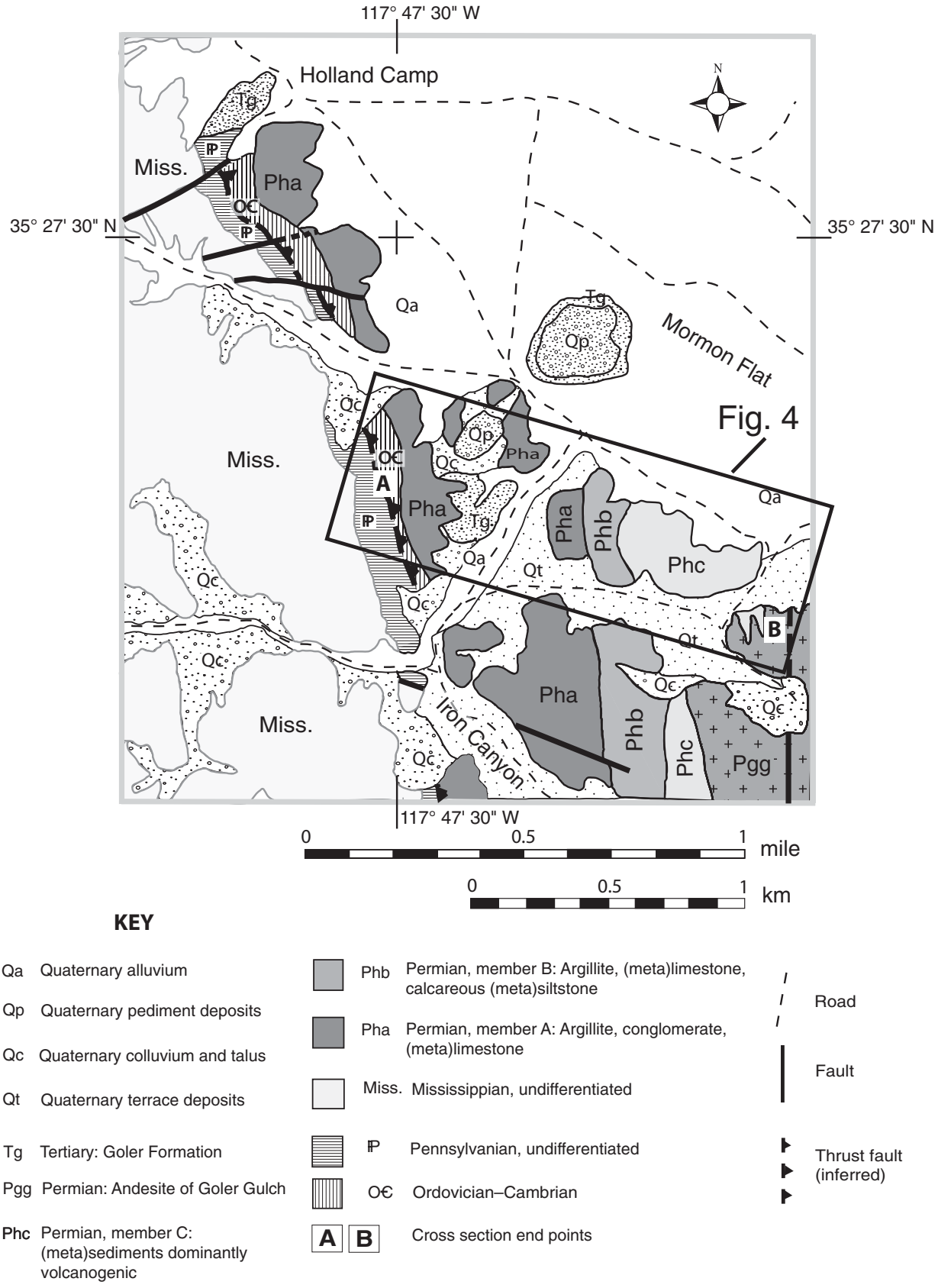

Figure 3. Geologic map of the study area and surrounding Paleozoic and Tertiary units, and location of cross section end points (see Fig. 4). Rock units are based on Carr et al. (1997). Cross section follows line of measured section between points A and B. Pha—member A, Phb—member B, Phc—member C.

Stevens et al., 2005; Miller et al., 1995). A slightly younger, earliest Triassic pluton (ca. 249 Ma) was emplaced into another part of the El Paso terrane in the southern Sierra Nevada (Dunne and Saleeby, 1993), whereas Early Triassic plutons in the northern Mojave Desert were emplaced into cratonic lithosphere (Martin and Walker, 1995).

Permian plutons in northern California and Nevada are thought to have originated as island arcs that were later accreted to the continental margin (Dickinson, 2000; Arvisu et al., 2009). In contrast, Permian plutons identified in NW Sonora, Mexico, and the El Paso Mountains, California, were associated with subduction along the continental margin (Fig. 1) (Miller et al., 1995; Barth et al., 1997; Arvisu et al., 2009). Regionally, Mesozoic and Cenozoic magmatism and deformation have removed or obscured volcanic records in the northern Mojave Desert and southern Sierra Nevada. The late Early Permian pluton in the El Paso Mountains appears to be uniquely associated with a preserved Permian sedimentary and volcanic rock record.

Paleozoic rocks of the El Paso Mountains were deposited in a marine setting (see references in Carr et al., 1997). The oldest Upper Cambrian to Devonian metasedimentary rocks originated as deep-marine fine-grained clastic sediments, chert, and limestone (Carr et al., 1984); they have been described as outer continental rise facies and correlated with similar coeval facies at Miller Mountain, west-central Nevada (Stevens et al., 2005). Overlying Mississippian through Permian metasedimentary rocks are calcareous to siliceous, consisting of meta-limestone, meta-argillite, meta-sandstone, and meta-conglomerate. Permian bioclastic meta-limestone components may be derived from the western North American carbonate shelf, the Bird Spring Formation (M.D. Carr, 2008, personal commun.). Two beds of well-rounded meta-quartzarenite within the Permian volcaniclastic layers suggest continental affinities. The youngest Permian rocks in the range are volcaniclastic meta-sandstones and meta-andesitic lava flows intruding and capping the Permian metasediments (Carr et al., 1997). The Early Permian age of the metasedimentary rocks is constrained by microfossils (Dibblee, 1952, 1967; Carr et al., 1984). Younger age constraints are the U-Pb age of the meta-andesite (262 ± 2 Ma; Martin and Walker, 1995) and a Late Permian pluton (260 ± 5 Ma; Miller et al., 1995), which intrudes the Upper Cambrian to Devonian deep-marine rocks of the El Paso Mountains. To the west, the Late Permian pluton also intrudes the nearby Bond Buyer sequence of metasedimentary strata and interlayered Early Permian andesite (ca. 281 ± 8 Ma; Martin and Walker, 1995) of uncertain connection with metasedimentary strata of the central El Paso Mountains (Fig. 2).

The stratigraphy of the Pennsylvanian and Permian section in the El Paso Mountains records deposition across "structurally controlled" basins and highs, preceding the development of Permian andesitic magmatism (Carr et al., 1997). Facies relationships suggest links to coeval strata in the Death Valley region (Walker, 1988; Martin and Walker, 1995). This borderland-like topography (Stone and Stevens, 1984; Martin and Walker, 1995; Dickinson, 2000) has been linked tentatively to the Pennsylvanian–Permian(?) displacement of the El Paso Mountains terrane southward from the Antler orogenic belt, possibly along a strand of a cryptic transform/truncation fault (Carr et al., 1997, 1984; Snow, 1992; Dickinson, 2000; Stevens et al., 2005), prior to development of Permian andesitic magmatism (Carr et al., 1997; Stevens et al., 1997).

As the El Paso Mountains basin records the onset of arc volcanism, it may be described as a pre-arc continental margin basin that evolved into an arc-related basin once magmatism began. Although the exact setting (forearc, intra-arc, backarc) is somewhat equivocal given the small outcrop area, fossil content shows that the basin remained marine up until the eruption of extensive lava flows.

Estimates of later tectonic displacement of the succession vary from ~30 km (Miller et al., 1995) up to a possible ~100 km (Stevens et al., 2005). Late Permian SW-vergent thrusting associated with emplacement of a Late Permian pluton occurred before emplacement eastward onto the cratonic platform in Triassic or Jurassic time (Miller et al., 1995). Regionally, Early Permian contractional deformation in the Inyo Mountains and conglomeratic deposition both there (Stevens et al., 1997; Stone et al., 2009) and in the El Paso terrane of the Kern Plateau (Dunne and Suczek, 1991) appear to have occurred contemporaneously with uplift in the El Paso Mountains. Martin and Walker (1995) also correlated deformation and Upper Permian–Lower Triassic strata in the northern Mojave Desert with uplift and volcanism in the El Paso Mountains.

Local Structural Setting

Late Permian contractional tectonism and accompanying regional metamorphism affected all Paleozoic strata in the El Paso Mountains, but evidence is not present in younger rocks (Carr et al., 1997). Southwest-vergent thrust faults, overturned tight to isoclinal folds of many scales, and penetrative and spaced cleavage developed throughout the range during this event. The study area lies within a thrust-fault–bounded, ~2-km-thick, stratigraphically upright panel of rock that appears to be among the least metamorphosed and deformed in the range. Metamorphic grade in the central part of the range, including the study area, is of the quartz-albite-muscovite-chlorite subfacies of the greenschist facies (Christiansen, 1961).

Strata in the study area have been mildly affected by both macroscopic and outcrop-scale, gently north-trending folds and by penetrative ductile deformation. Abrupt changes in amount of eastward dip along the traverse reflect the likely presence of a few large, open, kink-like flexures that are shown schematically in Figure 4. No axial-planar cleavage is associated with these folds. Carr et al. (1997) depicted similarly oriented, although more rounded folds in a cross section drawn ~750 m south of that in Figure 4. Outcrop-scale kink folds were noted in Cambrian–Ordovician strata near the west end of the study traverse, but not in traverse strata themselves. These kink folds deflect bedding and the bedding-parallel cleavage that is thought to have originated during the regional SW-vergent tectonism, and thus are younger than that tectonism. Very mildly developed penetrative (slaty) and spaced cleavage—the latter expressed by dissolution seams—is present in the study area. The two cleavages are approximately parallel to bedding and to each other, which is a common arrangement in east-dipping upright sections throughout the range (M. Carr, 2011, personal commun.), and this pattern is lithologically controlled. In some but not all outcrops, pebbles in conglomerate are slightly flattened into bedding planes.

One major and several minor faults are present adjacent to and along the study traverse. The east-dipping fault that underlies the study area (Fig. 4) was inferred by Carr et al. (1997) to be a significant thrust fault, although no definitive evidence for this sense of slip was presented, nor was any observed during the present study. Meaningful assessment of stratigraphic throw of the fault is impossible because the fault obliquely transects formations in both footwall and hanging wall as well as a regional mid-Paleozoic angular unconformity that removed significantly different amounts of strata in different locations. Faults characterized by stratigraphic separations of a few meters or less were noted at a few locations along the traverse.

METHODS

Field Methods

West and south of Mormon Flat (Figs. 3, 4, and 5), 985 m of strata were measured using a combination of Jacob staff, tape and Brunton, and a handheld Garmin eTrex global positioning system (GPS). This measured section extends across the thickest, most nearly homoclinal, and

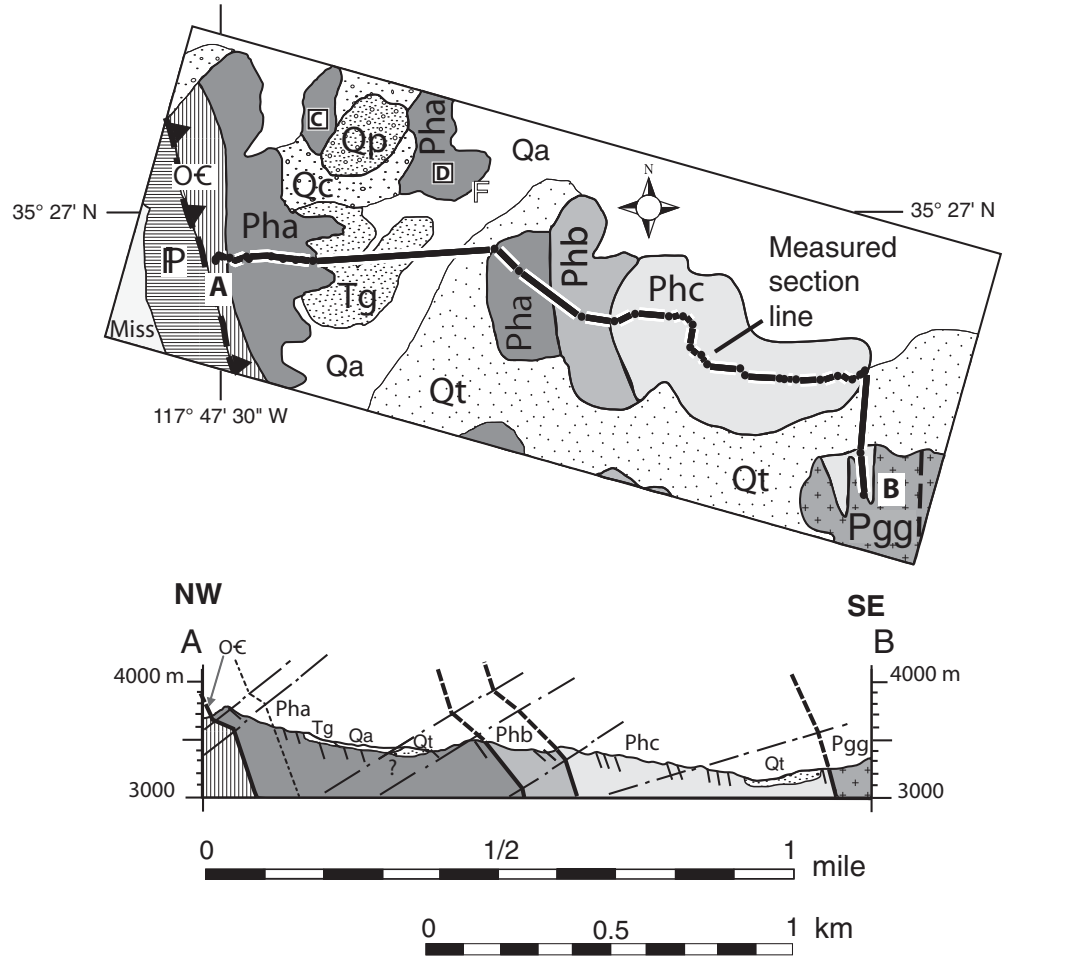

KEY

Qa	Quaternary alluvium	Pha	Permian, member A: Argillite, conglomerate, (meta)limestone		Appparent dip of bedding
Qp	Quaternary pediment deposits	Miss.	Mississippian, undifferentiated		Kink hinge plane
Qc	Quaternary colluvium and talus	IP	Pennsylvanian, undifferentiated		Arbitrary form surface
Qt	Quaternary terrace deposits	O€	Ordovician–Cambrian		Member contact (dashed in air)
Tg	Tertiary, Goler Formation	A B	Cross section end points		Inferred thrust fault
Pgg	Permian: Andesite of Goler Gulch	C D	Additional Pha sample areas, described in text		
Phc	Permian, member C: Metasediments, dominantly volcanogenic	F	*Nereites* ichnofossil location		
Phb	Permian, member B: Argillite, (meta)limestone, calcareous (meta)siltstone				

Figure 4. Close-up of study area of Figure 3, showing location of section measured from Ordovician–Cambrian (O€) deep-marine strata (point "A") through Permian metasedimentary strata (Pha/member A, Phb/member B, Phc/member C) to Permian andesite (Pgg) (point "B"). Section line is constrained by global positioning system coordinates (Rains, 2009). Measurements and samples were also taken from outcrops in portions of member A labeled "C" and "D." Approximate location of marine abyssal trace fossil "*Nereites*" is labeled "F." Cross section follows line of measured section between points A and B.

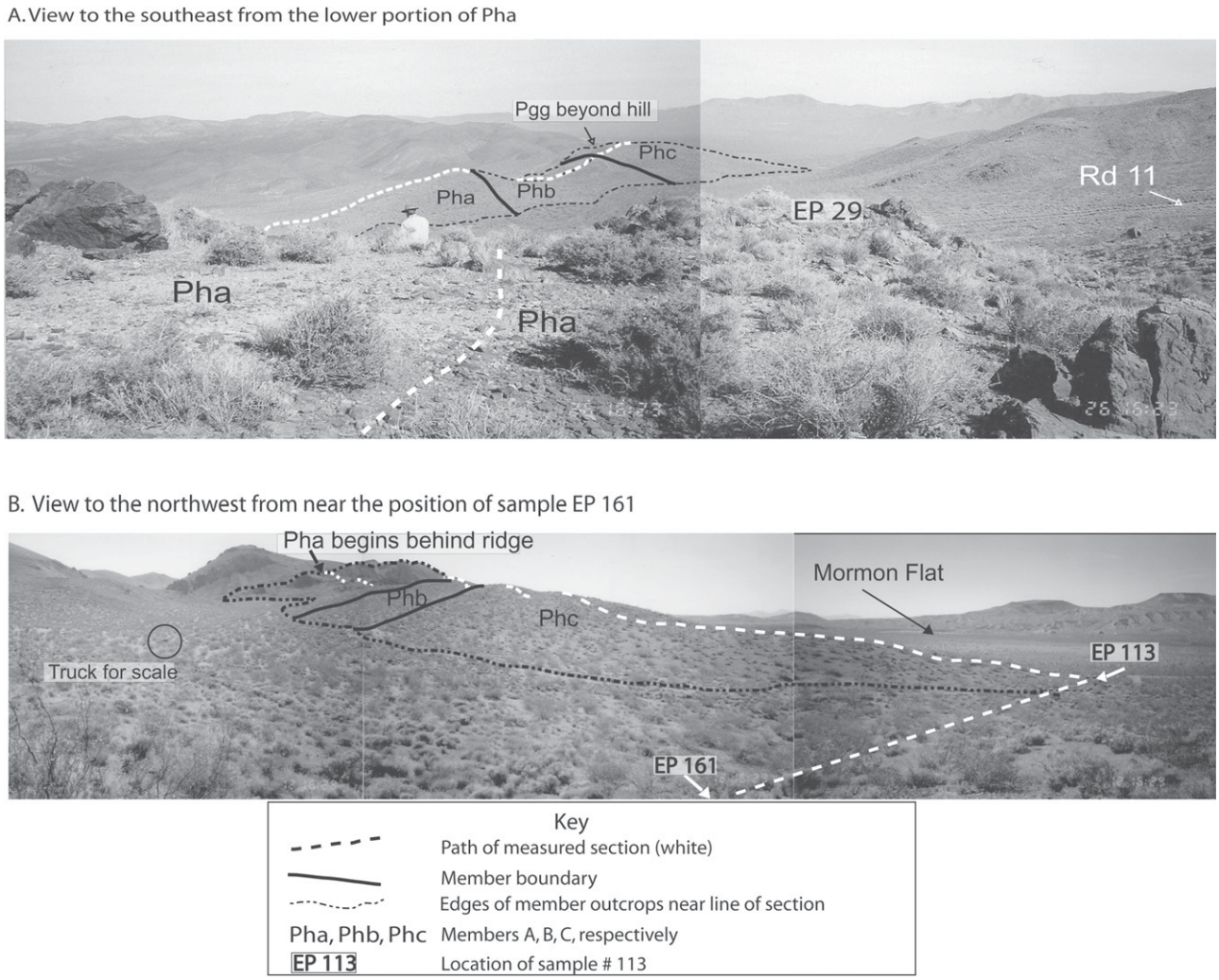

Figure 5. Photos of field area in El Paso Mountains. Dashed white line indicates path of measured section, although entire path is not visible in these photos. Dotted black line indicates edges of outcrops near section line; Quaternary sediment covers low-lying areas. Permian informal metasedimentary members are member A (Pha), member B (Phb), and member C (Phc). Pgg denotes overlying Permian andesite. Terms were adapted from Carr et al. (1997). Truck for scale in lower photo. EP "29," etc., refer to sample numbers.

apparently intact section of Permian metasedimentary and metavolcanic rocks, as mapped by Carr et al. (1997), i.e., the so-called "metasedimentary rocks of Holland Camp." It extends from the unconformable basal contact with Ordovician–Cambrian rocks to the conformable contact with overlying Upper Permian andesitic flows.

Carr et al. (1997) divided these strata into three members, based on lithology and conodont and fusulinid biostratigraphy; this informal terminology has been generally adapted for this study. The lowest, member A (Pha), is late Wolfcampian (ca. 280 Ma) to early Leonardian; the middle, member B (Phb), is late Wolfcampian and Leonardian; and the base of the upper portion, member C (Phc), is latest Leonardian (ca. 270.6 Ma). Phc is capped by the andesite of Goler Gulch (Pgg) with U-Pb zircon ages of 262 ± 2 Ma (Martin and Walker, 1995).

Lithologic and sedimentary features are summarized in a measured stratigraphic column (Figs. 6 and 7). One hundred-and-fifteen representative hand samples were taken at regular intervals in the measured section; selected sample locations were recorded as GPS waypoints using the North American Datum of 1983. Shallow excavations in covered intervals did not reveal the presumably less resistant material (argillite?) beneath, so these rocks are described as "covered" in the stratigraphic column.

Laboratory Methods

For more precise determination of lithologies via petrographic analysis, thin sections were made from 92 of the hand samples for petrographic description. Fifteen feldspar-bearing thin sections were stained for differentiation of plagioclase and potassium feldspar using the method outlined in Marsaglia and Tazaki (1992).

Twenty representative thin sections were point-counted for modal analysis using the Gazzi-Dickinson method (Dickinson et al., 1983; Ingersoll et al., 1984; Dickinson, 1985). The number of points counted varied according to sample grain size: as few as 100 points for a very coarse (meta) sandstone to granule (meta)conglomerate, and between 300 and 500 points for (meta)sandstone. Counted categories and recalculated parameters are defined in Table 1. Only detrital modes are presented here; petrographic point-count data were presented in Rains (2009), as were data from the

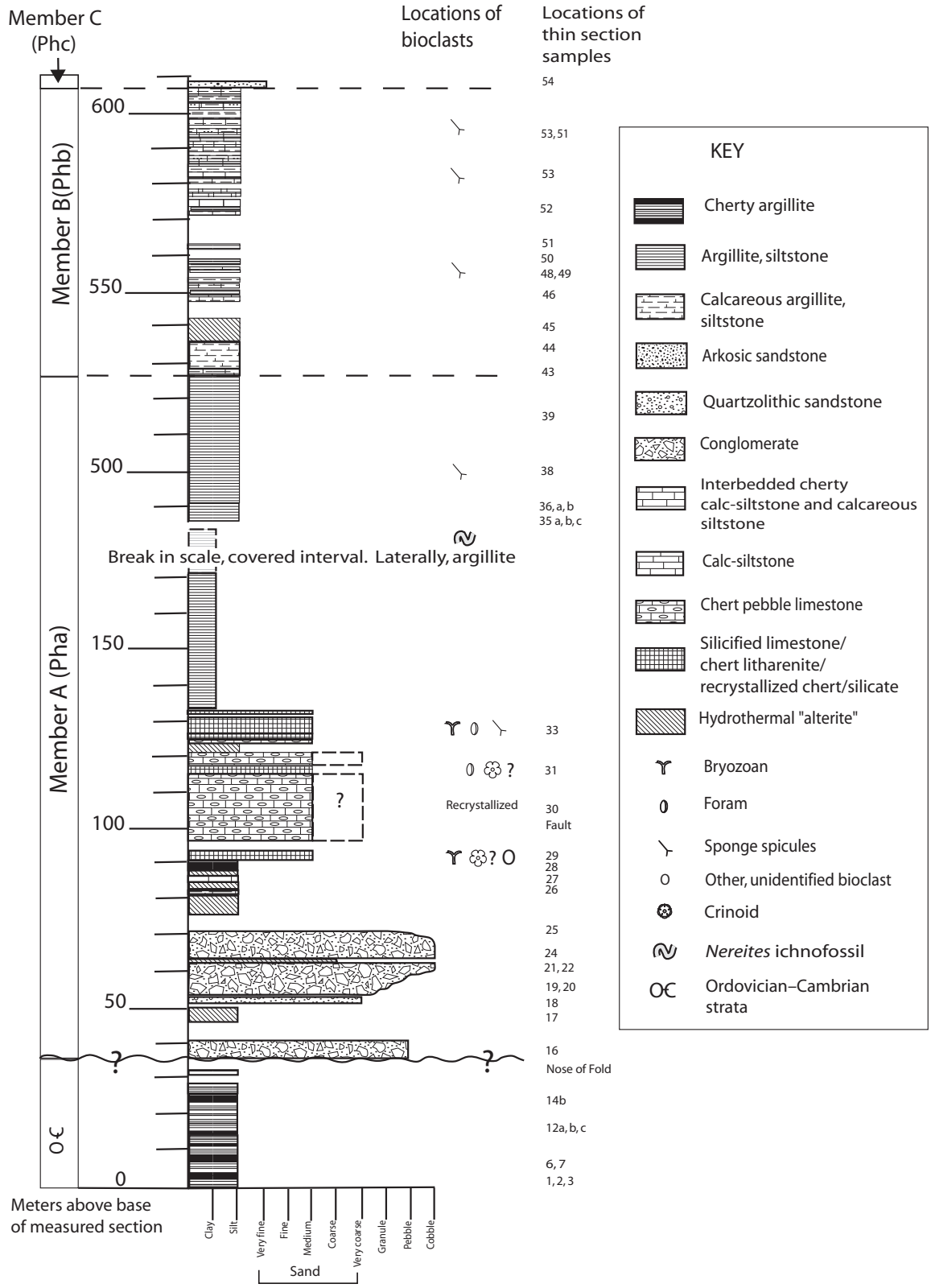

Figure 6. Stratigraphic column from 0 to 600 m above base of measured section. Includes the Ordovician–Upper Cambrian base, and the lower two Permian informal members, member A (Pha) and member B (Phb). Sponge spicules were found in calcareous beds of member A and member B and in sandy siltstone at the top of member A; other bioclasts were found only in silicified limestones. Trace fossils were found in one bed of member A, but in an outcrop offset laterally, north of the measured section, as noted in Figure 4 caption. Outcrops lateral to the large covered section of member A reveal argillite beds. Abyssal trace fossils are present in one layer, as noted in Figure 4.

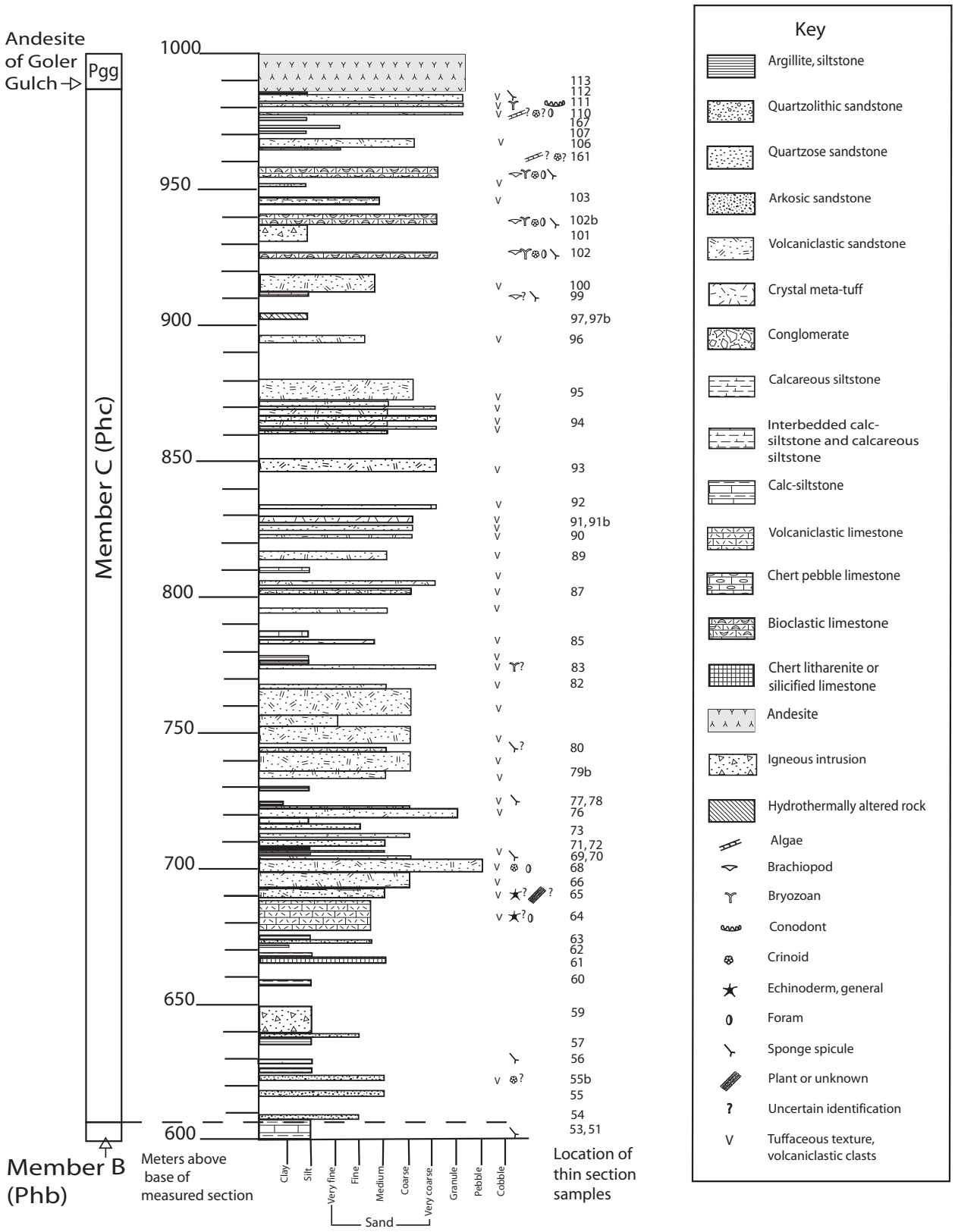

Figure 7. Stratigraphic column for section from 600 m to 985 m above base. Most of this portion of the measured section contains volcaniclastic metasediments and belongs to informal Permian member C (Phc). A greater variety of bioclasts is present in member C than in member A and member B, although a 100 m section between ~812 m and ~912 m contains neither marine bioclasts nor metacarbonate beds. A small interval containing unique beds of supermature meta-quartz sandstone occurs between ~705 and ~716 m; well-rounded quartz grains are almost entirely lacking in the rest of the measured section. The measured section is capped by meta-andesite.

TABLE 1. COUNTED AND RECALCULATED PARAMETERS

Counted parameters	
Qm	Monocrystalline quartz
Qp	Polycrystalline quartz
Qpch	Polycrystalline quartz (chert)
Qpch micro	Microcrystalline chert
Qpch rad	Radiolarian chert
Qpch spic	Spicular chert
Qpch silty	Silty chert
P	Plagioclase feldspar
P alt	Altered plagioclase feldspar
K	Potassium feldspar
Lvu	Volcanic lithic, undifferentiated
Lvl	Volcanic lithic with lathwork texture
Lvml	Volcanic lithic with microlitic texture
Lvv dvf	Volcanic lithic, devitrified glass
Lvv ves	Volcanic lithic, devitrified vesicular glass
Lss	Silicic sedimentary lithic
Lm	Metamorphic lithic
Lsc	Carbonate sedimentary lithic
Bio	Bioclast, siliceous or carbonate
B	Biotite
M	Muscovite
D	Dense minerals
Amph alt	Altered amphibole(?)
Other	Other, unknown
Matrix	Matrix, clay minerals (locally recrystallized)

Recalculated parameters
Qt = Qm + Qp + Qpch
Qpch = Qpch micro + Qpch rad + Qpch spic + Qpch silty
F = P + P(alt) + K
Lv = Lvu + Lvl + Lvml + Lvv dvf + Lvv ves
Lsm = Ls + Lm
L = Lv + Lsm
Lt = L + Qpch
QtFL%Q = 100*Qt/(Qt + F + L)
QtFL%F = 100*F/(Qt + F + L)
QtFL%L = 100*L/(Qt + F + L)
QpLvLsm%Qp = 100*Qp/(Qp + Lv + Lsm)
QpLvLsm%Lv = 100*Lv/(Qp + Lv + Lsm)
QpLvLsm%Lsm = 100*Lsm/(Qp + Lv + Lsm)

measured section, GPS waypoints, details of thin-section observations, point-count data, and additional sandstone modal-analysis ternary plots.

RESULTS

Measured Stratigraphic Section

Overall, the section appears stratigraphically intact, although subjected to low-grade metamorphism up to greenschist facies (Carr et al., 1997). However, much original mineralogy can be determined from relict textures, mineral remnants, and pseudomorph shapes. For the purposes of modal analysis, interpretation of original mineralogy was emphasized. Determining metamorphic mineralogy would have required detailed X-ray diffraction studies, which were beyond the scope of this project. Therefore, protolith terminology is used in descriptions and discussion hereafter.

Outcrops of the thin-bedded to massive-bedded strata are variably exposed along the line of section (Fig. 4). Conglomerate forms dark, desert-varnished ridges up to 5 m high. Beds of carbonate, sandstone, silicified limestone, and a section of interbedded siltstone and very fine-grained sandstone form smaller ridges. Isolated beds of siltstone and argillite have more subtle profiles. Beds are commonly laterally discontinuous, owing to variable exposure, and variable in thickness. Throughout the study area, outcrops are locally offset by small (~5–10 cm) faults. Consistent with Carr et al. (1997), no large fold hinges were observed in the study area. However, given the presence of cleavage, measured thicknesses are likely not original stratigraphic thicknesses.

The 985 m of sedimentary strata in the measured section (Figs. 6, 7, and 8) include 38 m of Ordovician–Upper Cambrian argillite and cherty argillite at the base, overlain by 947 m of moderately well-exposed Permian strata. However, Tertiary and Quaternary alluvium covers 315 m of the Lower Permian section. The top of the measured section ends at a stream cut that abuts a large outcrop of Quaternary alluvium (Fig. 4), so the line of section was laterally offset to the nearest exposed contact between the Permian sedimentary strata and the overlying andesite. Owing to the irregular nature of the contact between the Permian sedimentary and volcanic rocks and the trend of bedding, there may be some minor repetition of material included in the upper part of the measured section. The stratigraphic section extends 9 m into the overlying andesite flows. These are associated with hypabyssal intrusions near the top of the sedimentary section.

Overall, exposures of Permian metasedimentary strata in the measured section consist of 28% argillite and siltstone, 5% nonvolcaniclastic sandstone, 25% volcaniclastic sandstone, 5% conglomerate, 21% nonvolcaniclastic limestone, 3% volcaniclastic limestone, 3% silicified limestone and partially recrystallized chert, 4% hydrothermally altered intervals, and 6% younger, less-altered igneous intrusions of indeterminate age. Apart from the stream cut, covered intervals between outcrops make up 39% of the measured section. If all of these less resistant, covered intervals were interpreted as argillite, the overall percentage of argillite in the section would be 67%.

Lithologic Descriptions

Fine-grained facies. Within the measured section, variably calcareous argillite and siltstone outcrops make up 51% of member A (Pha), 33% of member B (Phb), and 7% of member C (Phc) (Fig. 8). As also noted by Carr et al. (1997), these very fine-grained sedimentary rocks are thinly to massively bedded, laterally uneven in thickness, and commonly fissile. Fresh rock faces vary from gray to light bluish gray to brownish gray, weathering to light brown. Parallel bedding and lamination are found throughout. In member A (Pha) and member B (Phb), this lithology is commonly exposed in continuous sections; however, in member C (Phc), thin-bedded shale and siltstone layers fine up from, or are interbedded with, more thickly bedded sandstone.

Petrographic analysis shows that several samples from the three members are composed of subequal amounts of carbonate and silica. Much of the siliceous material is recrystallized sponge spicules; carbonate is also recrystallized. These rocks were classified as calcareous siltstones or as calc-siltstones, depending on the relative abundance of siliceous versus calcareous components. In thin section, some argillite and siltstone samples show faint to distinct laminations and local bioturbation(?). Diagenetic effects include stylolites in clay-rich zones.

Most of the fine-grained siliceous facies in member A (Pha) are carbonate-free argillite and siltstone. Uncommon laminated calcareous argillite, light-gray weathering to light brown in outcrop, is found in the lower part of member A, where it is interbedded with carbonate strata. A thick section of light-gray to reddish-brown fissile argillite characterizes the middle of member A. Outcrops of member A lateral to the line of section that crosses the large covered interval (Fig. 4) were found also to be fissile argillite. At least one bed contains *Nereites* ichnofossils. In thin section, the reddish-brown argillite exhibits finely disseminated iron oxides

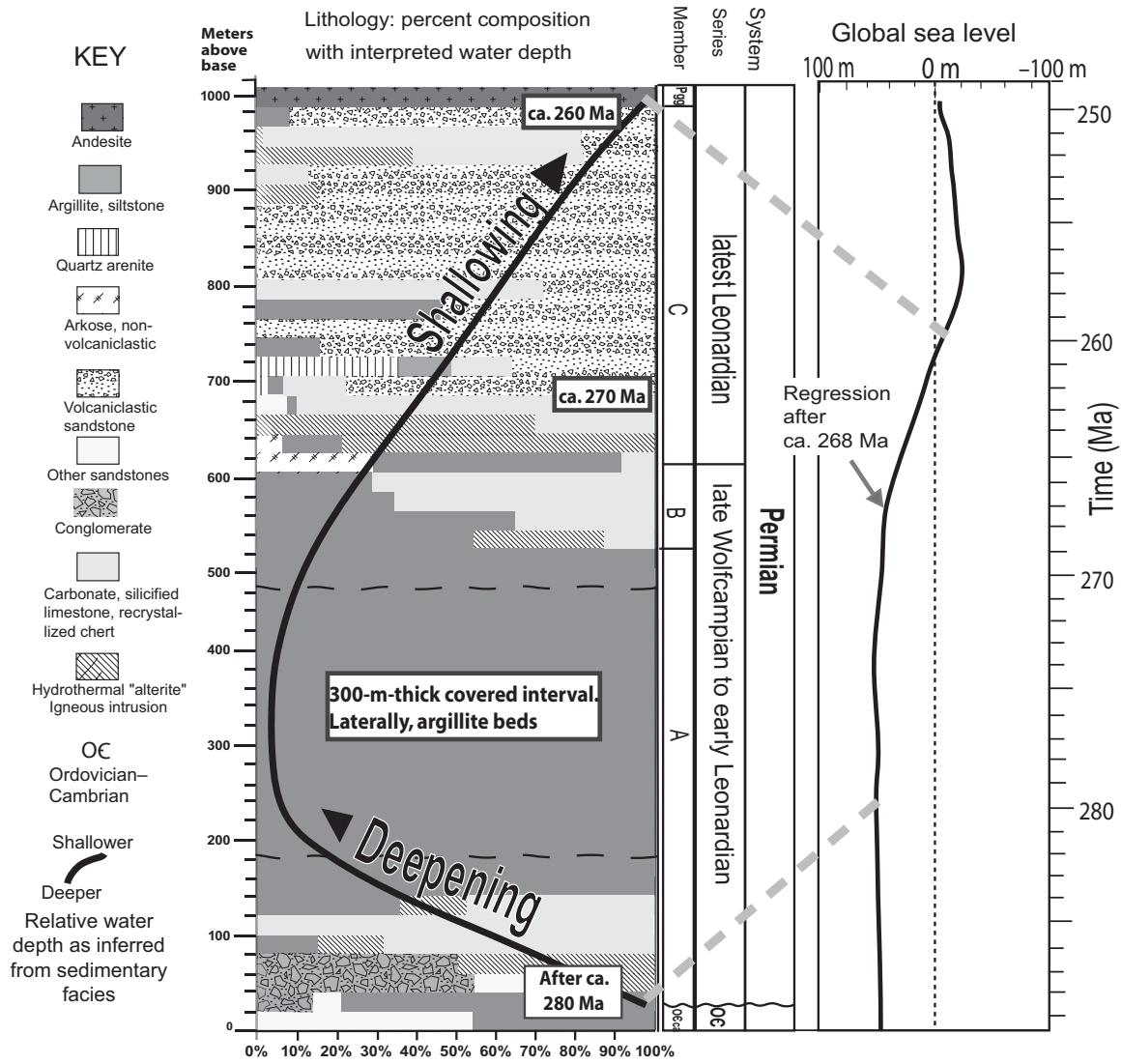

Figure 8. Vertical column on left shows relative percentages of lithologies (0%–100%) in 20 m slices from the base to the top of measured section, normalized to 100% for each 20 m. Member A (Pha), is dominated by sandy meta-conglomerate, meta-carbonate, and meta-siltstone. The sandy conglomerate in Pha lacks marine bioclasts and may have been deposited subaerially. Member B (Phb) contains meta-carbonate and meta-siltstone. The base of member C (Phc) is defined by the occurrence of plagioclase-rich arkosic rocks and is dominated by volcaniclastic rocks throughout, with an interval of rare supermature meta-quartz sandstone, and local interbeds of meta-carbonate. Top of measured section is meta-andesite. Age constraints are: lower member A, ca. 280 Ma; lower member C, ca. 270 Ma (Carr et al., 1997); capping andesite, 262 ± 2 Ma (Martin and Walker, 1995); and 260 ± 5 Ma for the intruding Permian pluton (Miller et al., 1995). The interpreted water depth of deposition of El Paso Mountains strata is compared to the Permian global sea-level curve from Haq and Schutter (2008). The global sea-level curve shows a rise relative to the baseline (dotted line at 0 m) for positive (left) and a fall for negative (right) values. Superposed on vertical column is an El Paso Mountains (EPM) relative sea-level curve (thick line) based on distribution of shallow versus deep-water facies. The El Paso Mountains water depth changes, based on strata interpretation, are one to two orders of magnitude greater than global sea-level variation and out-of-phase with global sea-level changes for the early deepening trend at ca. 280 Ma, so the depositional environments are a consequence of vertical tectonics (see text).

in a recrystallized mud matrix. Iron-stained grayish-orange, laminated to thinly bedded argillite to sandy siltstone beds form a continuously exposed section near the top of the member. In thin section, one sample contains very angular to well-rounded, fine- to very fine-grained chert lithic fragments (~20%), quartz grains (~7%), angular to subangular opaque grains (~7%), and trace sponge spicules, set in a cherty-silty clay matrix (~60%) with patchy calcite cement. The opaque minerals define lamination.

Member B (Phb) is more calcareous than member A (Pha) and consists of thinly to thickly bedded, medium- to dark-gray argillite and medium-gray to yellowish-brown calcareous argillite interbedded with dark-yellowish-orange calc-siltstone. Covered intervals between outcrops are more extensive than in member A (Pha). In thin section, all samples from member B (Phb) consist of clay or silt with local sponge spicules, and opaque, (organic?) material.

In member C (Phc), the few exposures of argillite and siltstone are concentrated in the lower half and the very top of the member. Beds are dominantly very thick, with a few thin beds near the base and top of the member. Parallel lamination was observed in two beds. Thin sections of samples from this interval showed diverse lithologies: (1) calcareous siltstone with subequal amounts of siliceous and carbonate silt; (2) cherty argillite with minor (<5% of the rock) lithic clasts of spicular chert and siltstone; (3) volcaniclastic siltstone containing very fine-grained plagioclase and quartz grains; and (4) siltstone from the top of the member, distinguished from the other argillites in member C (Phc) by the presence of dark (organic?) material.

Quartzolithic and quartzose sandstone. Exposures of quartzolithic and quartzose sandstone are sparsely distributed throughout the measured stratigraphic column; they appear to make up ~3% of member A (Pha), ~0% of member B (Phb), and ~5% of member C (Phc).

In member A (Pha), quartzolithic (cherty) sandstone occurs near the base, where conglomerate fines up to thinly bedded, pale-blue to desert-varnished grayish-black, coarse-grained sandstone. In thin section, the sandstone is very poorly sorted and similar in grain composition to conglomerates, containing angular to subrounded clasts of chert, dominantly radiolarian, but also spicular and silty. Uncommon siltstone fragments are present. Silty matrix ranges from 1% to 5%, and there is some local quartz cement.

In member C (Phc), several unique beds of brownish-gray to light-olive-gray, thickly to massively bedded sandstone have a sugary appearance in hand sample. In thin section, they are composed of well-rounded, moderately sorted (bimodal), medium-grained monocrystalline quartz grains cemented by quartz and calcite (Fig. 9E). Grain contacts are point, long, and sutured. These quartzarenite layers are unusual in this stratigraphic section because their only framework grains are monocrystalline quartz; also present are ~1% –2% of grains of unknown primary mineralogy replaced(?) by carbonate.

Plagioclase-rich arkosic and volcaniclastic sandstone. Plagioclase-rich arkosic and volcaniclastic sandstone, where the dominant sandstone framework grains are plagioclase, are limited to member C (Phc). These grains are universally altered to some extent and locally completely replaced (pseudomorphed) by authigenic/metamorphic minerals (Figs. 9D, 10A, 10C, and 10D). Notably, no potassium feldspar was observed in these sandstones. Plagioclase-rich arkosic sandstone in the basal 60 m of member C comprises ~3% of the unit and has only trace amounts of possibly volcaniclastic components, as opposed to the more volcaniclastic-rich sandstone in the overlying 300 m of member C (Phc), which has variably altered plagioclase grains and volcaniclastic lithic fragments in an altered matrix. Alteration varies among the samples, with plagioclase grains and volcanic lithic fragments being more easily discerned in less-altered samples.

In outcrop, plagioclase-rich arkosic sandstone beds are medium to very thick bedded, very fine or medium grained, and very light gray, weathering to pale yellowish orange. Locally, the arkose is white-speckled greenish gray, thickly bedded, and medium to coarse grained. The finer-grained samples are more matrix rich (up to ~20%), more altered, and dominated by subrounded to rounded, untwinned and unzoned altered plagioclase with common angular to subangular quartz grains and uncommon bipyramidal zircon in one sample. Altered plagioclase grains are difficult to distinguish from a cherty matrix that may consist of devitrified volcanic glass shards. Some matrix, since it has the same distribution and size as other grains, may be pseudomatrix composed of compacted mudstone lithic fragments. Rarely, quartz grains appear resorbed (Figs. 4A, 5B, and 9D) and/or well rounded. Trace amounts of lithic fragments include limestone, siltstone, chert, and microlitic volcanics (Fig. 10A). Also present are calcite and hematite cements, and evidence of compaction.

Volcaniclastic sandstone composes ~61% of the middle and upper section of member C (Phc). It is very thickly to massively bedded and dominantly greenish gray and less commonly bluish gray or yellowish brown. Black to white clasts give some samples a speckled appearance in hand specimen. In thin section, tuffaceous sandstones are generally medium to very coarse grained, and very poorly to moderately sorted. Clasts are predominantly subangular to subrounded. Distinguishing characteristics of volcaniclastic sandstones include the dominance of angular to subrounded, uncommonly zoned, commonly twinned plagioclase grains and/or plagioclase pseudomorphs surrounded by altered clay-calcite-opaque matrix. Plagioclase varies in degree of alteration/replacement by sericite and carbonate from ~20% to 100%. Even when completely altered, pseudomorphed plagioclase exhibits relict shape, twinning, and zoning (Figs. 10C, 10D, and 10E).

Lithic clasts in the volcaniclastic sandstones are dominantly subangular to rounded volcanic fragments with uncommon zoned or twinned plagioclase crystals, which are variably altered or pseudomorphed (Figs. 10A, 10C, and 10D). In thin section, the composition of volcanic lithic fragments appears similar to the composition of the general matrix of the sandstones, with a similar ratio of plagioclase grains to groundmass. Volcanic lithic clasts can be distinguished from the matrix by the presence of clay or iron-oxide rims on the clasts or differences in interior plagioclase crystal size. In several samples, grain alteration to clay minerals/sericite obscures boundaries between clasts and matrix. In other samples, iron-oxide alteration is present within the sandstone matrix but not within the volcanic-lithic-fragment groundmass, helping to distinguish the two. The two stratigraphically highest volcaniclastic sandstones show pseudomorphs of vesicular glass in thin section (Fig. 10F). Other rare to common lithic components are chert and sedimentary clasts along with rare carbonate clasts. The rare carbonate clasts observed in thin section are likely intrabasinal, since they either contain volcaniclastic plagioclase crystals or were deposited near the top of the section, where bioclast type suggests shallower water depths. Some "chert" lithics are locally abundant and were likely derived from devitrified volcanic glass.

Monocrystalline quartz grains are present in trace amounts in most member C volcaniclastic sandstone. They are generally angular-subangular to subrounded, but three of the thin sections from the top of the section exhibit a bimodal suite of angular and rounded monocrystalline quartz. One sample has traces of well-rounded monocrystalline quartz that may be silicified biogenic debris, possibly radiolaria.

Trace amounts of altered biotite and muscovite appear in ~60% of the samples studied from member C. Similar amounts of pseudomorphed amphibole(?), distinguished by its crystal form and reaction rims, are present in a few samples (Fig. 10B).

Bioclasts are found in volcaniclastic sandstone both near the base and the top of member C (Figs. 9C and 9F). Bioclasts in the lower 75 m of member C include sponge spicules and fragments(?), echinoderm fragments, bryozoan fragments, foraminifers, and unknown grains, including possible plant debris (Fig. 9F). Bioclast types in the upper 80 m of member C include algae(?), brachiopod, bryozoan, conodont(?), crinoids, and foraminifer fragments (Figs. 9C and 9F).

Matrix makes up ~20% to 80% of sandstone samples. Some samples show more compaction than others, with abundant seaming parallel or subparallel to layering in the matrix around plagioclase grains and volcanic lithics. Cherty areas within the matrix of some samples are possibly fragments of devitrified volcanic glass.

Two samples are especially pyroclast-rich, their composition being dominantly plagioclase (or pseudomorphs) and uncommon altered amphibole(?) crystals set in ~60%–80% matrix with a volcaniclastic texture, including some relict bubble shards. These tuffs(?) have the same general

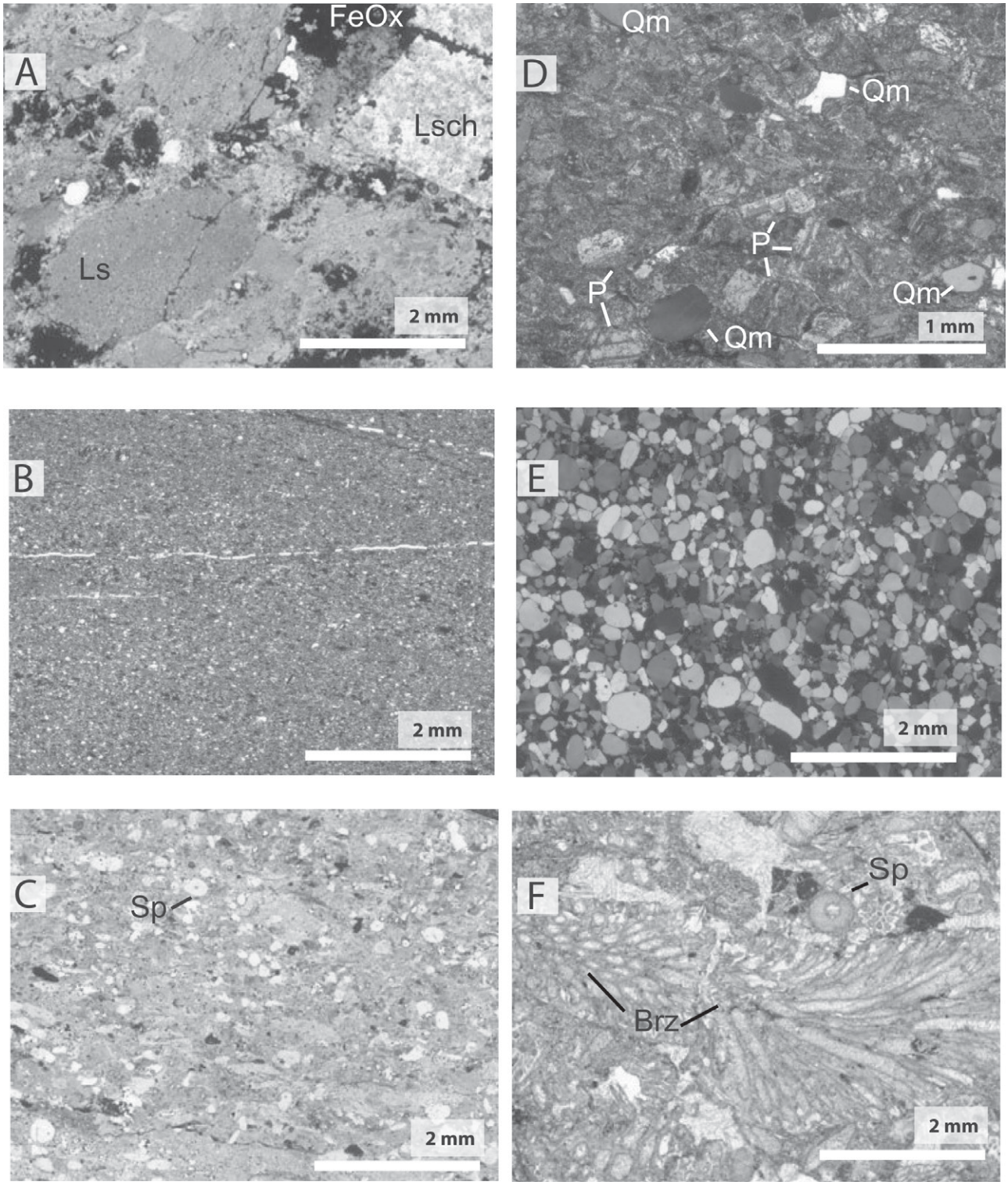

Figure 9. Photomicrographs of various rock types. (A) Member A, sample EP 16, chert meta-conglomerate, plane light. Rounded to angular clasts of chert (Lsch), variably silty, and argillite (Ls). Matrix appears similar to clasts and is partially recrystallized. Alteration to iron oxides (FeOx) is pervasive in matrix and along fractures. Other fractures through grains are cemented by quartz. (B) Member A, sample EP 34, reddish argillite, plane light. Silt-size quartz and opaque grains are evenly disseminated. Fractures in the sample are filled with quartz cement. (C) Member A, sample EP 38, plane light. A slightly coarser sample of argillite from the upper portion of member A contains chert and angular quartz in burrowed(?) clay (smectite?) matrix. Sp—sponge spicule. (D) Member C, sample EP 55, plagioclase-rich arkose, nicols crossed. Image shows plagioclase grains (P), many twinned, and monocrystalline quartz (Qm). Matrix and grains are heavily altered to iron oxide. (E) Member C, sample EP 71, calcite-cemented quartzarenite, nicols crossed. (F) Member C, sample EP 102b, limestone, plane light. Very coarse-grained bioclastic packstone, the most coarse-grained carbonate layer in the measured section. Sp—sponge spicule, Brz—bryozoan.

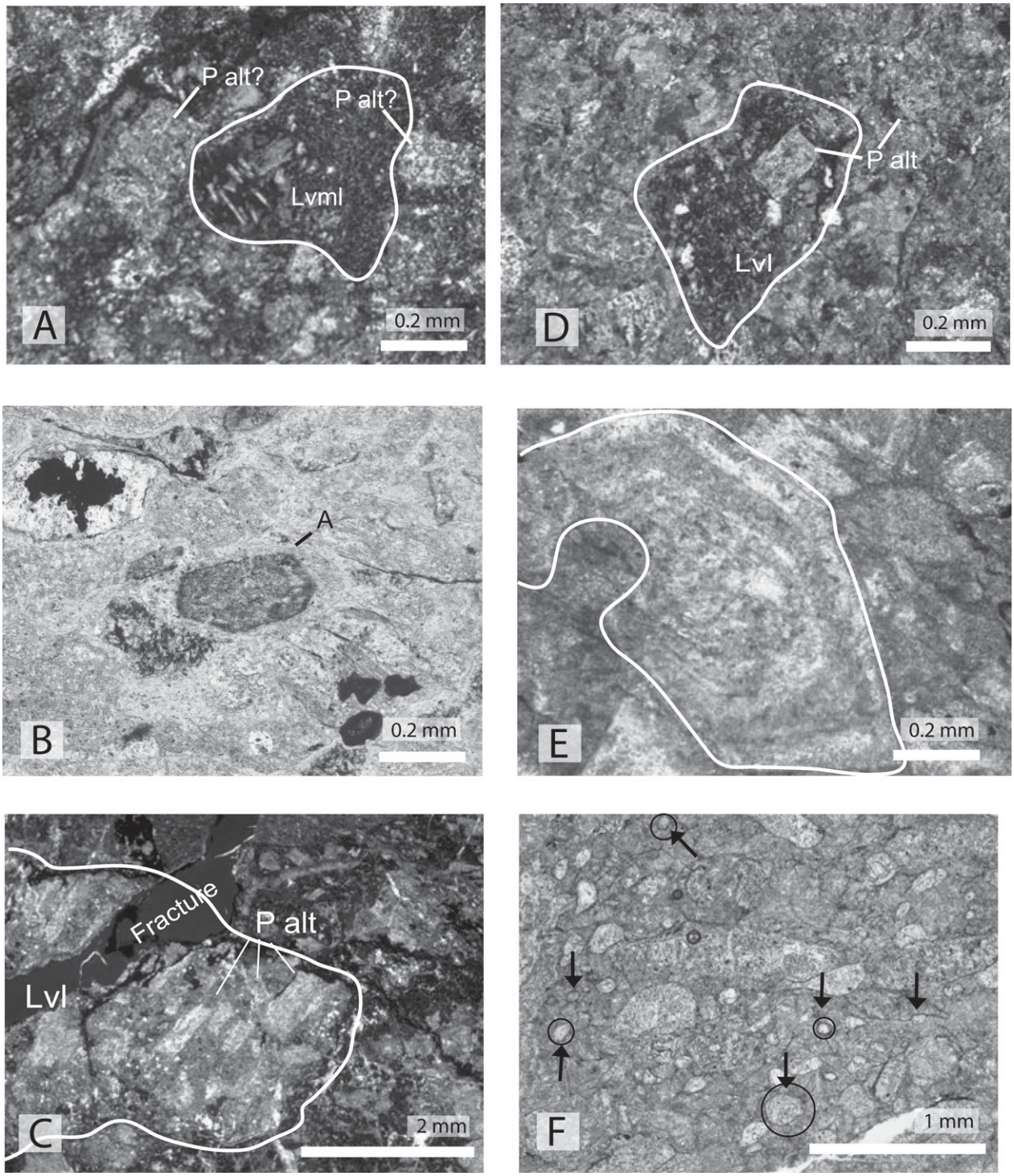

Figure 10. Various photomicrographs of member C. (A) Sample EP 55b, plagioclase-rich arkose, nicols crossed. Matrix shows both "cherty" areas and carbonate. "Chert" material may be devitrified volcanic glass, as discussed in text. Small darker grain in the center appears to be a volcanic lithic clast with microlitic texture. "P alt" indicates possible altered plagioclase(?). Lvml—Volcanic lithic with microlitic texture. (B) Sample EP 65, calcareous cherty volcaniclastic sandstone, plane light, from base of volcaniclastic section. "A" indicates a possible altered amphibole. Dark areas are due to presence of opaque alteration minerals. (C) Sample EP 66, calcareous volcaniclastic sandstone, nicols crossed. Volcanic lithic clast with lathwork texture (Lvl). Matrix containing plagioclase crystals is altered to iron oxides; this helps to differentiate lithic clasts from the plagioclase-rich matrix. A fracture separates parts of lithic clast. (D) Sample EP 77, calcareous volcaniclastic sandstone, nicols crossed. In center is a volcanic lithic clast, Lvl, with an apparently devitrified volcanic glass matrix making up most of the clast. Rest of field of view shows altered plagioclase crystals in a carbonate matrix. Plagioclase crystals are partially altered to carbonate. (E) Sample EP 69, volcaniclastic sandstone, plane light. A partially altered plagioclase grain (outlined) shows euhedral shape, oscillatory zoning, and embayment. (F) Sample EP 111, calcareous volcaniclastic sandstone, plane light. This sample from near the top of the measured section appears to show carbonate-filled vesicular glass remnants; arrows and/or circles indicate some vesicles.

appearance and degree of alteration as the volcaniclastic sandstone, yet they have little or no nonvolcanic clasts (e.g., sedimentary clasts or bioclasts). These samples contain the highest percentage of matrix, suggesting that they were originally poorly sorted.

Conglomerate. Thickly to massively bedded conglomerate comprises ~11% of member A (Fig. 8). Outcrops of conglomerate are light gray and weather to light brown; desert varnish gives a splotchy dark appearance to the conglomerates from a distance. Conglomeratic outcrops form ridges up to 5 m high. Beds of conglomerate are laterally uneven in thickness and appear somewhat amalgamated. In some outcrops, layering 2–10 cm thick is suggested by variations in average size of tan to dark-gray gravel clasts that range up to cobble size; there are also some laminated sandy interbeds. Massive layers 2 m to 3 m thick include a coarse-grained matrix with both rounded and disc-shaped pebbles and cobbles.

Thin sections of four conglomerate samples revealed them to be very poorly to poorly sorted, consisting dominantly of very angular to well-rounded granules to pebbles (Fig. 9A). Clasts are dominantly chert and argillite and also include trace amounts of polycrystalline quartz and sandstone composed of well-rounded monocrystalline quartz grains. The chert clasts are commonly radiolarian bearing, also spicular, or silty. Coarse-grained angular to subrounded monocrystalline quartz grains are common or occur in trace amounts. Contacts between clasts are commonly long or sutured. Silt to sand cherty matrix generally ranges in abundance from ~1% to ~20%, but is up to ~70% in more altered(?) or more poorly sorted(?) samples.

Limestone and silicified limestone. Limestone in members A, B, and C is dominantly very thickly to massively bedded, light-gray to orange weathered calc-siltstone, although a few thinner beds are present. Variations include pale-yellowish-brown cherty layers in member A, several greenish-gray to bluish-gray to yellowish-brown volcaniclastic beds in member C, and several beds of moderate-dark-gray cherty bioclastic packstone near the top of the section in member C. Interbedded with cherty limestone in member A, there are layers of thickly to massively bedded, medium-gray to dark-yellowish-orange, partially recrystallized silicified limestone, and coarse-grained, light-gray to light-brown, partially brecciated, partially recrystallized chert. A similar partially recrystallized silicified limestone layer is located near the base of member C. Limestone beds are more abundant in the lower two members, A and B, than in member C.

Most samples of calc-siltstone in members A and B, and the lower part of member C (below the first volcaniclastic bed) lack bioclasts in thin section. Rare to common bioclasts in member C include sponge spicules and silicified foraminifers, bryozoan(?), and crinoid(?) fragments. One sample in member B is ~50% siliceous-sponge-spicule silt and ~50% calcareous silt.

Several limestone beds in member C are volcaniclastic, with variable amounts of zoned plagioclase, partly replaced by carbonate, and altered clasts (volcanic glass?). The stratigraphically highest volcaniclastic carbonate rock contains rounded plagioclase silt, trace amounts of biotite, sponge spicules, and other unidentified bioclast fragments in a calcareous silt matrix.

The remainder of the nonvolcaniclastic limestone in member C consists of thickly to massively bedded, cherty, coarse-grained bioclastic packstone. There are angular chert granules; bryozoan and sponge(?) bioclasts are visible with a hand lens. In thin section, fragments of brachiopods, bryozoans, sponges, foraminifers, and crinoids are present; some carbonate bioclasts are partially silicified (Fig. 9F).

Hydrothermally(?) altered rocks and igneous intrusions. Hydrothermally(?) altered sedimentary and/or igneous intrusive rocks are present in all three members, but their character varies among the members, with unidentifiable sedimentary protoliths and undetermined mineralogies. In member C, as previously described by Carr et al. (1997), both altered sedimentary layers and unaltered post-Permian igneous intrusions are present.

Andesite. Andesite exposure is poor in the study area. In thin section, the andesite is dominantly composed of very fine- to medium-grained, euhedral to subhedral, plagioclase crystals. Groundmass containing fine opaques composes ~30% to ~40% of the rock and is partially altered to chlorite.

From samples taken ~1 km to the east of the study area, M.D. Carr (2008, written commun.) described the dominant volcanic rock as an andesite porphyry, with plagioclase laths ranging from a few percent to ~80% of the rock. The remainder of the andesite is a very fine-grained matrix of "plagioclase, minor quartz, and opaque minerals," along with up to 10% hornblende. Alteration minerals are chlorite and iron oxide. Lesser components of the extrusive and hypabyssal volcanic rocks are "medium-grained hornblende-pyroxene quartz diorite to diorite."

DISCUSSION

Broad Stratigraphic Trends and El Paso Mountains Basin History

Stratigraphic trends and the history of the El Paso Mountains basin are based on the interpretation of lithology, fossil content, and sandstone detrital modes in the section studied during this investigation. Depositional environments of the three informal members in this study of the El Paso Mountains (members A, B, and C) are primarily marine, based on fossil content, with the possible exception of the local basal conglomerate of member A. Facies variations indicate changing relative water depth and depositional environments through time that could be a consequence of local tectonic or eustatic effects. Published Permian global sea-level curves show a fairly constant level from ca. 300 to 260 Ma, with a gradual fall in global sea level starting at ca. 260 Ma (Haq and Schutter, 2008). Thus, we interpret sea-level changes implied by facies analysis of the Permian stratigraphic sequence in the El Paso Mountains to be a product of tectonic rather than eustatic controls (Fig. 8). Hence, in the following discussion, we use the terms "subsidence" and "uplift."

Above an unconformable contact with underlying Ordovician–Cambrian hemipelagic sedimentary rocks, the local base of the Permian section is marked by a distinct conglomerate. The abundant chert and cherty argillite clasts, perhaps originating from rocks similar to the underlying Paleozoic deep-marine units, implies tectonism, uplift, and subaerial exposure of deep-marine rocks in the source area, perhaps a local tectonic high. Rounded clasts indicate likely subaerial origin and transport, but lithification and metamorphism preclude detailed shape analysis to determine whether they are more likely of fluvial or beach origin. Sandstone detrital modes are similar to those associated with subduction complex or fold-and-thrust belt provenance, an interpretation that is consistent with a tectonically uplifted source (Figs. 11 and 12). The basin then deepened, or the source of the coarse clastics was shut off, as evidenced by overlying very fine-grained carbonate and hemipelagic sediments. Further deepening below the carbonate compensation depth (CCD) is suggested by an overlying interval of carbonate-free, fine-grained, red mudstone to siltstone.

The depth of the CCD is dependent on factors such as water temperature, dissolved CO_2, and salinity (Berger et al., 1976, 1981). Permian deposition occurred at low latitudes, ~10°N (Tabor and Montañez, 2002), and equatorial sea-surface temperatures may have been similar to those of today (Kiehl and Shields, 2005), suggesting CCD depths similar to the present equatorial average of 5500 m. However, modeling of Middle Permian conditions indicates that CO_2 levels were about four times higher than at present (Winguth et al., 2002), suggesting shallower CCD levels, perhaps 4500 or 3500 m. Although local coastal conditions may affect the

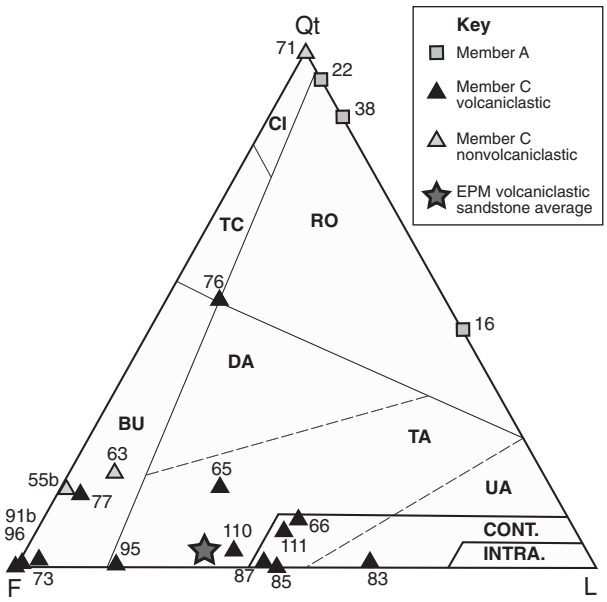

Figure 11. Ternary plot (Qt-F-L) of point count data. Sand provenance fields are from Dickinson (1985). Sand provenance: CI—craton interior, TC—transitional continental, BU—basement uplift, RO—recycled orogen, DA—dissected arc, TA—transitional arc, UA—undissected arc (Dickinson, 1985). INTRA.—intraoceanic arc, and CONT.—continental arc, showing maximum mean values for QtFL%Qt in intraoceanic and continental arcs (Marsaglia and Ingersoll, 1992). Sample numbers are located next to square and triangle symbols. Most member C samples plot outside of the magmatic-arc provenance fields of Dickinson (1985) and Marsaglia and Ingersoll (1992). (See Rains [2009] for discussion of diagenetic effects on the composition of the volcaniclastic sandstones.) Note that samples EP 55b and EP 76 contain very few grains so that QtFL percentages have large errors. Average of El Paso Mountains (EPM) volcaniclastic sandstone does not include samples EP 55b and EP 63, as they are feldspathic, but not volcaniclastic.

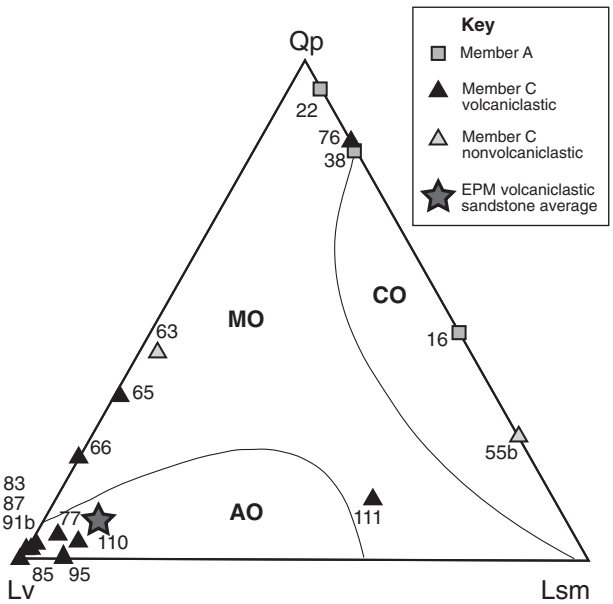

Figure 12. Ternary plot (Qp-Lv-Lsm) of point-count data emphasizing lithic components. Qp—chert lithic clasts, Lv—volcanic and metavolcanic lithic clasts, Lsm—sedimentary and metasedimentary lithic clasts. MO—mixed orogen, AO—arc orogen, CO—collision orogen. Provenance fields are from Dickinson (1985).

CCD, given the low latitude of the El Paso Mountains terrane in the Permian and the likely influence of the shelfal carbonate platform, subsidence below the CCD is a reasonable interpretation of the stratigraphy. Above the carbonate-free argillite, the presence of carbonate beds, including bioclastic turbidites among hemipelagic layers in member B, suggests some slight decrease in water depth (above CCD?). Although carbonate shelf sediment may be carried by gravity flows and deposited below the CCD (e.g., Nichols, 1999), the subsequent increase in coarse clastic input in member C is consistent with a shallowing trend.

The base of member C (608 m above the local base of the measured section) is defined by the presence of medium- to very thick-bedded, moderate- to well-sorted, plagioclase-rich arkose, where it is locally interbedded with lithologies similar to those in member B, suggesting an influx of coarser sediment. Possible sources of the plagioclase grains may be translated crustal blocks along a proposed truncation fault (Fig. 1) or derivation from earlier nearby(?) magmatism, represented by the Bond Buyer sequence roof pendant in the western El Paso Mountains (Fig. 2) (281 ± 8 Ma; Martin and Walker, 1995). The lack of zoning in the plagioclase in these rocks differentiates them from the overlying volcaniclastic sandstones, but we cannot rule out a local volcanic source.

The oldest disseminated volcaniclastic debris occurs at ~678 m above the base of member A in a very thick interval of cherty calcarenite, and it is the first direct indication of local volcanic activity in this section; thick volcaniclastic beds in the overlying ~90 m contain a varying mix of poorly to very poorly sorted, subangular to subrounded, volcaniclastic, calcareous and chert clasts. The overlying dominance of thick-bedded volcaniclastic sandstone is consistent with deposition on a submarine volcanic-arc apron, as described by Smith and Landis (1995). Very coarse-grained bioclastic limestone beds near the top of the column suggest shallowing of the basin, owing to rapid filling by volcanic debris or perhaps uplift prior to intrusion and extrusion of the capping andesite flows. This is further evidence for the growth of an intermediate volcanic edifice. Carr et al. (1997) noted that the exposed andesite comprised flows and flow breccia without pillow structures, leaving the depositional setting (marine/nonmarine) equivocal.

Relating Basin History to Subduction Initiation Modeling

We chose the El Paso Mountains study area because it appeared to have a complete stratigraphic record of magmatic-arc development, but as we have outlined herein, it also may record subduction inception along the southwestern U.S. margin. We now compare this record to stratigraphy predicted by numerical modeling of subduction initiation by Gurnis et al. (2004) and Cenozoic records of subduction initiation (e.g., Gurnis et al., 2004; Stern, 2004; Sutherland et al., 2006). These studies imply that the sedimentary record of "induced" subduction initiation in a proto-forearc would begin with rapid uplift (subaerial), followed by rapid subsidence, and then shallowing (Fig. 13). Cenozoic sedimentary records of subduction initiation along Puysegur Ridge, New Zealand, referenced in the modeling, also show an ongoing sedimentary pattern of rapid uplift, rapid subsidence, and then shallowing (Gurnis et al., 2004; Sutherland et al., 2006). In contrast, "spontaneous" subduction initiation should result in a sedimentary pattern of initial subsidence and magmatism in the proto-forearc (Stern, 2004; Marsaglia, 2012).

Numerical modeling by Gurnis et al. (2004) indicates that "induced" subduction initiation requires a through-going fault or lithospheric break such as a transform fault or ridge, buoyancy contrast across the fault (Niu et al., 2003), and development of compressive tectonics before progressing to self-sustaining subduction. In the Permian, the underlying lithosphere in the El Paso Mountains was likely associated with transitional continental crust (outer continental rise; Stevens et al., 2005), and therefore was

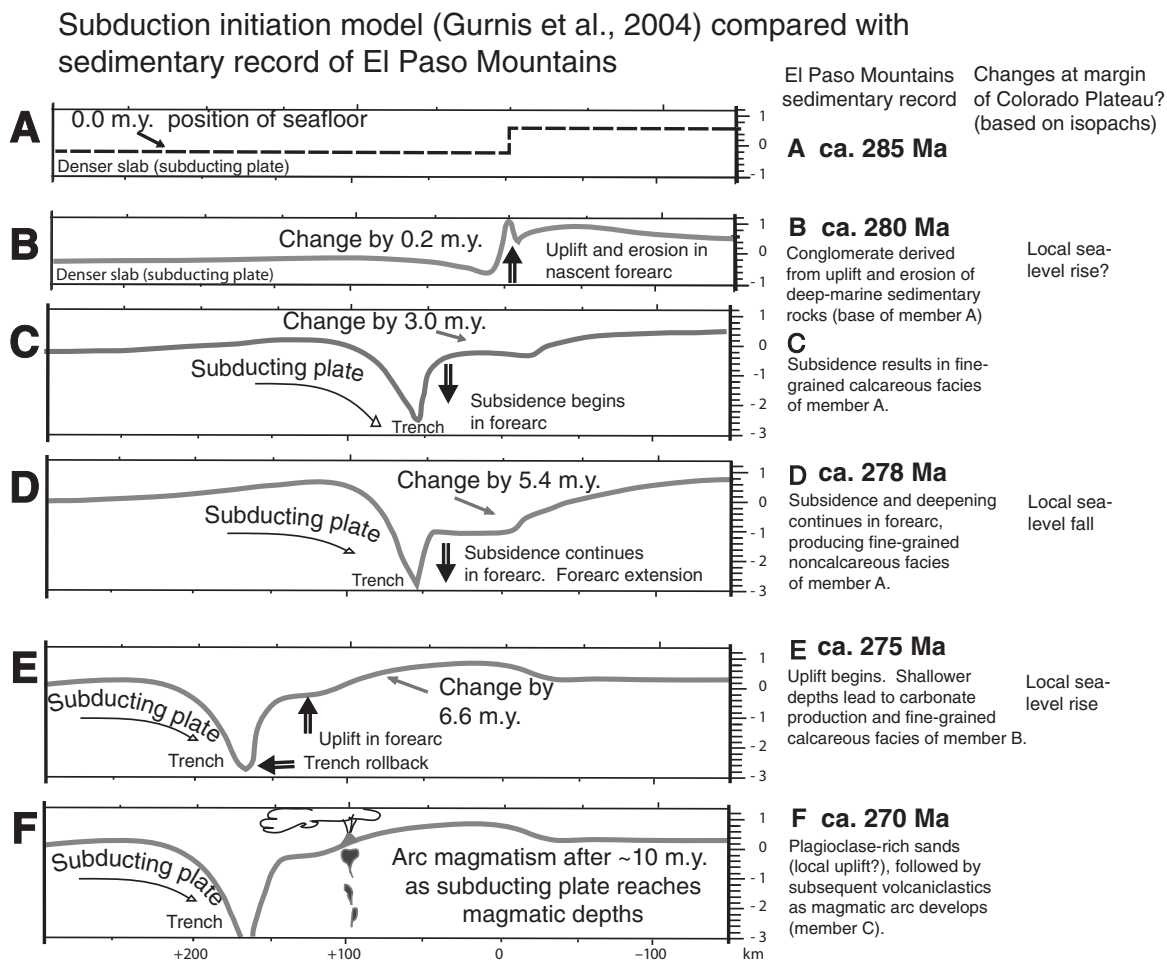

Figure 13. Evolution of subduction initiation based on dynamic modeling (Gurnis et al., 2004; Hall et al., 2003) using example of an oceanic fracture zone with crustal density differences across a zone of weakness. Figure is adapted from Gurnis et al. (2004) and Hall et al. (2003); position of plates is reversed for this adaptation. Compression is given as 2 cm/yr, and plate ages in the model are 10 m.y. (right, younger) and 40 m.y. (left, older). Time spans (0.0, 0.2, 3.0, 5.4, 6.6 m.y.) are based on modeling. (A) Juxtaposition of oceanic lithosphere with age/density differences across fracture zone/zone of weakness, as described in text. (B) Initial compression deforms overriding slab. (C–D) Forearc subsidence occurs as the plates decouple (Gurnis et al., 2004). (E) Overriding slab moves trenchward. Vertical motion is relative to ocean floor; models are consistent with data from Cenozoic ocean arcs (Gurnis et al., 2004). In adapting model to the El Paso Mountains (EPM) on right, the "younger" plate of model is equated with underlying, less dense, transitional continental-margin lithosphere of the El Paso Mountains terrane. Subducting plate is assumed to be denser oceanic lithosphere. Note that vertical motions of forearc region in model follow the same pattern as that interpreted from the Permian sedimentary record in the El Paso Mountains. Furthermore, far-field effects at right edge of model may be comparable to patterns of transgression and regression as recorded in sedimentary isopachs of the western Colorado Plateau (based on isopach compilations by Zahler, 2006; see Fig. 1).

more buoyant than subducting oceanic crust and lithosphere. As described already, some authors have suggested the El Paso terrane was translated from northern California and left behind on a sliver of the postulated late Paleozoic transform/truncation fault (e.g., Stevens et al., 2005; Dickinson, 2000). Alternatively, as mentioned already, if the Antler belt extended to what is now central California, little or no latitudinal translation of the El Paso Mountains terrane may have occurred in the Pennsylvanian or Permian (Dickinson, 1981; Stone, 1984; Carr et al., 1984; Snow, 1992; Dunne and Saleeby, 1993; Stevens et al., 2005). In any case, it is proposed that left-lateral transform faulting brought oceanic lithosphere into juxtaposition with the El Paso Mountains terrane, enabling the necessary density contrast and creating an opportunity for subduction initiation along a through-going zone of weakness.

Looking only at southern California, the observed pattern of southwestern Cordilleran Permian–Triassic plutons, based on palinspastic reconstruction of Stevens et al. (2005), suggests that magmatism began in a small area (El Paso Mountains) before spreading south (Barth and Wooden, 2006) (Fig. 14). This pattern may be analogous to the Cenozoic initiation and propagation of subduction along the Puysegur Ridge, New Zealand, and consistent with the record of restricted nucleation and progression of volcanism along that margin (Sutherland et al., 2006).

The overall Permian sedimentary pattern of the El Paso Mountains appears consistent with models for "induced" or "forced" subduction initiation, rather than "spontaneous" subduction (Gurnis et al., 2004; Stern, 2004; Sutherland et al., 2006) (Fig. 13). Specifically, initial uplift is evidenced at the base of member A by sandy conglomerate, followed by a

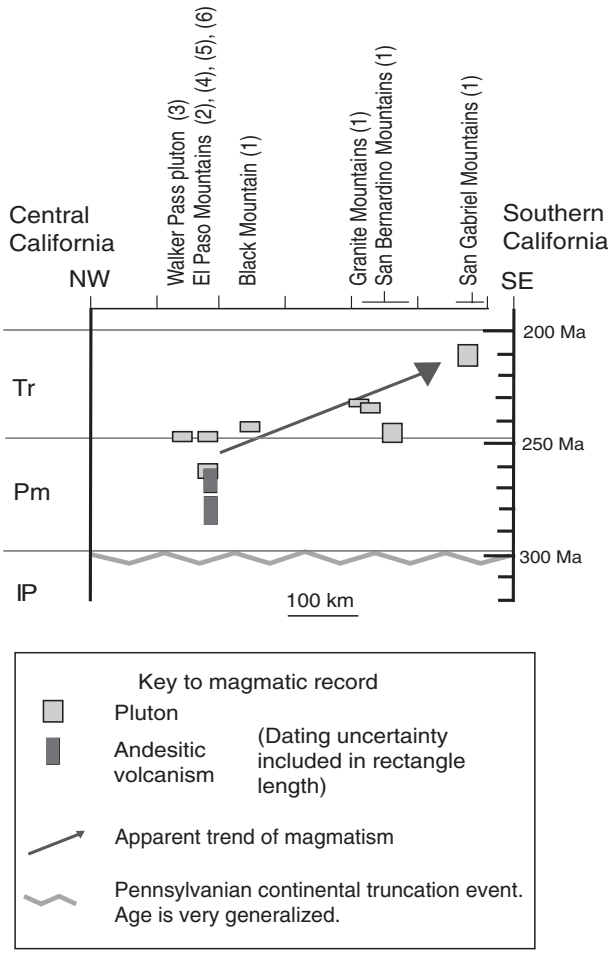

Figure 14. Magmatic activity from ca. 300 Ma to ca. 200 Ma between southernmost central California and southern California, given geographic locations based on Permian paleogeographic reconstruction of Stevens et al. (2005). Reconstructed locations are projected to proposed Pennsylvanian–Permian truncation fault line. Plotting of magmatic activity based on various studies suggests a trend from Permian initiation in or near the El Paso Mountains, with magmatism spreading in Triassic time. Later tectonic events south of the El Paso Mountains have removed volcanic cover, leaving only plutons to mark magmatic activity (Barth and Wooden, 2006). Bar in Pennsylvanian time is a generalized schematic of the truncation fault that cut across the continental margin (Stevens et al., 2005). References for magmatic activity: (1) Barth and Wooden (2006), (2) Carr et al. (1997), (3) Dunne and Saleeby (1993), (4) Martin and Walker (1995), (5) Miller et al. (1995), (6) interpretation from this study.

deepening marine sequence that suggests subsidence below the CCD. Deep-marine strata occur throughout member B, where renewed carbonate influx suggests progressive shallowing/uplift. Coarsening of sediment and increased carbonate at the base of member C are consistent with further shallowing. This shallowing trend was overprinted by input from the evolving magmatic arc, as first indicated by disseminated volcaniclastic debris near the base of member C, which then becomes more volcaniclastic-dominated upward, consistent with deposition on a prograding volcaniclastic apron. Very coarse-grained bioclastic limestone near the top of the measured section indicates a very shallow-marine setting prior to proximal magmatism (andesite intrusions and flows).

The time span of subduction initiation to magmatism in the Gurnis et al. (2004) model is less than 10 m.y. (Fig. 13). For the Permian section in the El Paso Mountains, the interval between the uplift of deep-marine rocks and the incursion of volcaniclastic sediments was also ~10 m.y.

Limited Permian subduction initiation in the southern California region contrasts with more extensive Triassic subduction development along the trace of the subsequent Mesozoic arc. Saleeby (2011) suggested that Triassic subduction followed latest Permian compressive tectonics along the oceanic transform-continental margin interface. His detailed study of remnants of the transform within the Kings-Kaweah ophiolite belt (KKO, Fig. 1) gives an age of ≥200 Ma; this transform would have resulted in a large density contrast between outer continental and negatively buoyant transform oceanic lithosphere, i.e., conditions favoring subduction initiation in the Triassic along the length of the transform. However, in the Early Permian, as mentioned herein, a record of contraction occurring at the same time as uplift in the El Paso Mountains is found from the western El Paso terrane in the Kern Plateau (Dunne and Suczek, 1991) through the southern Inyo Mountains and vicinity (Stevens and Stone, 2007; Stone et al., 2009), supporting an earlier occurrence of perhaps "induced" subduction. We speculate that the localization of Permian subduction in the El Paso Mountain region and its apparent southward propagation were associated with a preexisting condition either associated with the lithospheric structure of the soon-to-be subducting oceanic plate (e.g., change in age/structure/thickness across a transform or fossil spreading or other aseismic ridge at that paleolatitude) or the presubduction geometry of the overriding plate (e.g., older indentation or jog associated with a prior tectonic regime).

Regional Ramifications of Subduction Initiation

Whereas we interpret the Permian sedimentary record of the El Paso Mountains to show a proximal sequence consistent with subduction initiation, it is also worth considering potential far-field effects, such as those discussed by Holford et al. (2009), and implied by geodynamic models (Gurnis et al., 2004) (Fig. 1), which may include shoreline migration on the craton and uplift of the Last Chance allochthon (e.g., Snow, 1992).

The numerical models imply that several-hundred kilometers inboard of the trench, on the overriding plate, the rock record would show subtle vertical changes at subduction inception, followed by more substantial subsidence as subduction resistance lessened (Fig. 13). Taking into account the removal of Basin and Range extension and shortening the distance, shoreline regression on the western edge of the Colorado Plateau between ca. 285 and ca. 278 Ma, as determined by sedimentary isopachs (Zahler, 2006, and sources cited within), may be reflecting the lithospheric flexure predicted by modeling (Fig. 1). Between ca. 275 Ma and ca. 270 Ma, both the El Paso Mountains and the Colorado Plateau show evidence of transgression/subsidence in opposition to global eustatic trends (Fig. 8) but consistent with vertical motions suggested by the geodynamic model of Gurnis et al. (2004).

SUMMARY AND CONCLUSIONS

Petrologic investigation of Permian metasedimentary rocks in the El Paso Mountains reveals a rock record indicating uplift (member A) and subsidence (member A, middle and top, and member B) before influx of volcaniclastic sediments and renewed shallowing (member C).

At the base of member A, upward-coarsening conglomeratic strata indicate uplift. A high-energy environment with variable flow energy is suggested by fairly large chert and argillite clasts and variable amounts of matrix. Sharp contacts, upward fining, and lack of sedimentary structures are consistent with gravity-flow deposits. Clast composition suggests derivation from deep-marine sedimentary rocks. However, the lack

of marine bioclasts means that the sedimentary environment was not conclusively marine.

The conglomeratic deposits are overlain by fine-grained turbidite facies (middle and top of member A and in member B) that indicate subsidence. Overlying the conglomeratic deposits, there are carbonate and siliceous layers (middle of member A), which are overlain by a carbonate-free layer (middle to the top of member A). Subsidence below the CCD is suggested by lack of carbonate beds and the red color of argillite layers. Abyssal depth is also suggested by *Nereites* ichnofossils (Prothero, 1998). In member B, the presence of fine-grained carbonate layers among hemipelagic beds suggests a relative decrease in water depth. A marine depositional environment is indicated by local marine microfossils.

Plagioclase-rich and volcaniclastic sediments dominate member C. At the base of member C, two intervals of plagioclase-rich arkosic sandstone interrupt the fine-grained sedimentary pattern. Carbonate beds are thicker up section below the volcaniclastic section. The first volcaniclastic influx, as indicated by rare plagioclase crystals in thickly bedded limestone, signaled the beginning of volcaniclastic input. Overlying layers in the middle to upper part of member C are dominated by plagioclase-rich strata, volcaniclastic sandstone, and resedimented tuffs, with local interbeds of quartzarenite, limestone, and uncommon interbeds of argillite. Layers are dominantly very thickly bedded to massive, parallel bedded, very fine to very coarse grained, and poorly to very poorly sorted, consistent with deposition on a volcanic apron. Intermediate magma composition is suggested by the dominance of plagioclase and sparse amphibole phenocrysts, similar to those in overlying andesite. Marine bioclasts within both volcaniclastic sandstone and local beds of limestone in the lower and upper sections of member C indicate a marine depositional environment. The dearth of volcaniclastic material in bioclastic packstone near the top of the section suggests development of a fringing reef or carbonate platform between eruptive events. The very coarse grain size of the packstone and vesicular remnants(?) in volcaniclastic sandstone near the top of the section suggest shallowing of the volcanic apron or filling of the volcanic basin.

When compared with numerical models and Cenozoic examples of subduction initiation, especially the Miocene to Holocene Puysegur Ridge–Fiordland subduction zone of New Zealand, the interpreted Permian sedimentary record of the El Paso Mountains—of uplift and subsidence followed by volcaniclastic sediment influx—is consistent with the pattern of a developing magmatic arc in a newly initiated subduction zone. Since the El Paso Mountains basin records the onset of arc volcanism, it may be described as a pre-arc continental margin basin that evolved into an arc-related basin once magmatism began. The exact setting (forearc, intra-arc, backarc) is somewhat equivocal, given the small outcrop area, but fossil content shows that it remained marine up until the eruption of extensive lava flows. Reported magmatic trends in central and southern California after ca. 285 Ma (Barth et al., 1997), using palinspastic Permian locations from Stevens et al. (2005), suggest that volcanism nucleated in or near the El Paso Mountains and then propagated southward (Fig. 14).

Subduction initiation modeling and Cenozoic oceanic arc records predict likely near-field and far-field effects in relative water depths for the overriding plate. Depositional environments in the three informal members of the study area of the El Paso Mountains are primarily marine, with the possible exception of the local conglomeratic base of member A. Stratigraphic variations in the Permian sedimentary rocks in the El Paso Mountains indicate changing relative water depths, consistent with predicted near-field effects. Global sea-level curves within the time frame of the Permian section (ca. 280 Ma to ca. 260 Ma) in the El Paso Mountains indicate that the inferred changing relative water depths were likely the result of regional tectonics, especially between ca. 280 Ma and ca. 267 Ma. Far-field effects may be reflected in coeval facies changes on the western edge of the Colorado Plateau and may be related to coeval uplift and basin formation in the Death Valley region and Last Chance allochthon as well. In the Colorado Plateau, facies show local variations in relative water depth; the pattern suggests crustal flexure associated with subduction initiation in the El Paso Mountains and may be consistent with predictions based on subduction initiation models.

ACKNOWLEDGMENTS

We thank Michael D. Carr for providing background information; this study depended in large part on work previously done by him and other investigators of the El Paso Mountains. Graduate research funds from the Department of Geology of California State University–Northridge helped support this work. We thank Richard Rains, Whitney Behr, and Kevin Rivera for field assistance. The manuscript was greatly improved by reviews by Ray Ingersoll and an anonymous reviewer, as well as comments from John Wakabayashi.

REFERENCES CITED

Arvisu, H.E., Iriondo, A., Izaguirre A., Chávez-Cabello, G., Kamenov, G.D., Solís-Pichardo, G., Foster, D.A., and Lozano-Santa Cruz, R., 2009, Rocas graníticas pérmicas en la Sierra Pinta, NW de Sonora, México: Magmatismo de subducción asociado al inicio del margen continental activo del SW de Norteamérica: Revista Mexicana de Ciencias Geológicas, v. 26, no. 3, p. 709–728.

Barth, A.P., and Wooden, J.L., 2006, Timing of magmatism following initial convergence at a passive margin, southwestern U.S. Cordillera, and ages of lower crustal magma sources: The Journal of Geology, v. 114, p. 231–245, doi:10.1086/499573.

Barth, A.P., Tosdal, R.M., Wooden, J.L., and Howard, K.A., 1997, Triassic plutonism in southern California: Southward younging of arc initiation along a truncated continental margin: Tectonics, v. 16, no. 2, p. 290–304, doi:10.1029/96TC03596.

Berger, W.H., Adelseck, C.G., and Mayer, L., 1976, Distribution of carbonate in surface sediments of the Pacific Ocean: Journal of Geophysical Research, v. 81, p. 2617–2627, doi:10.1029/JC081i015p02617.

Berger, W.H., Vincent, E., and Thierstein, H.R., 1981, The deep-sea record: Major steps in Cenozoic ocean evolution, *in* Warme, J.E., Douglas, R.G., and Winterer, E.L., eds., The Deep Sea Drilling Project: A Decade of Progress: Society of Economic Paleontologists and Mineralogists Special Publication 32, p. 489–504.

Burchfiel, B.C., and Davis, G.A., 1972, Structural framework and evolution of the southern part of the Cordilleran orogen, western United States: American Journal of Science, v. 272, p. 97–118, doi:10.2475/ajs.272.2.97.

Burchfiel, B.C., and Davis, G.A., 1975, Nature and controls of Cordilleran orogenesis, western United States: Extensions of an earlier synthesis: American Journal of Science, v. 275-A, p. 363–396.

Burchfiel, B.C., and Davis, G.A., 1981, Triassic and Jurassic tectonic evolution of the Klamath-Sierra Nevada geologic terrane, *in* Ernst, W.G., ed., The Geotectonic Development of California (Rubey Volume I): Englewood Cliffs, New Jersey, Prentice-Hall, p. 50–70.

Carr, M.D., Christiansen, R.I., and Poole, F.G., 1984, Pre-Cenozoic geology of the El Paso Mountains, southwestern Great Basin, California—A summary, *in* Lintz, J., Jr., ed., Western Geological Excursions: Reno, Nevada, Department of Geological Sciences, McKay School of Mines, v. 4, p. 84–93.

Carr, M.D., Christiansen, R.L., Poole, F.G., and Goodge, J.W., 1997, Bedrock Geologic Map of the El Paso Mountains in the Garlock and El Paso Peaks 7–1/2′ Quadrangles, Kern County, California: U.S. Geological Survey Miscellaneous Investigations Series Map I-2389, 9 p., scale 1:24,000.

Christiansen, R.L., 1961, Structure, metamorphism, and plutonism in the El Paso Mountains, Mojave Desert, California [Ph.D. thesis]: Stanford University, Stanford, California, 180 p.

Dibblee, T.W., 1952, Geology of the Saltdale Quadrangle, California: California Division of Mines and Geology Bulletin 160, 43 p.

Dibblee, T.W., 1967, Areal Geology of the Western Mojave Desert: U.S. Geological Survey Professional Paper 522, 153 p.

Dickinson, W.R., 1981, Plate tectonics and the continental margin of California, *in* Ernst, W.G., ed., The Geotectonic Development of California: Rubey Volume I: Englewood Cliffs, New Jersey, Prentice-Hall, p. 2–28.

Dickinson, W.R., 1985, Interpreting provenance relations from detrital modes of sandstones, *in* Zuffa, G.G., ed., Provenance of Arenites: Proceedings of the NATO Advanced Study Institute on Reading Provenance from Arenites, Cetraro, Cosenza, Italy, June 3–11, 1984: Hingham, Maine, Kluwer Academic Publishers, p. 333–361.

Dickinson, W.R., 2000, Geodynamic interpretation of Paleozoic tectonic trends oriented oblique to the Mesozoic Klamath-Sierran continental margin in California, *in* Soreghan, M.J., and Gehrels, G.E., eds., Paleozoic and Triassic Paleogeography and Tectonics of Western Nevada and Northern California: Geological Society of America Special Paper 347, p. 209–245.

Dickinson, W.R., 2006, Geotectonic evolution of the Great Basin: Geosphere, v. 2, no. 7, p. 353–368; doi: 10.1130/GES00054.1.

Dickinson, W.R., and Lawton, T.F., 2001, Carboniferous to Cretaceous assembly and fragmentation of Mexico: Geological Society of America Bulletin, v. 113, no. 9, p. 1142–1160, doi:10.1130/0016-7606(2001)113<1142:CTCAAF>2.0.CO;2.

Dickinson, W.R., Beard, L.S., Brakenridge, G.R., Erjavec, J.L., Ferguson, R.C., Inman, K.F., Knepp, R.A., Lindberg, F.A., and Ryberg, P.T., 1983, Provenance of North American Phanerozoic sandstone in relation to tectonic setting: Geological Society of America Bulletin, v. 94, p. 222–235, doi:10.1130/0016-7606(1983)94<222:PONAPS>2.0.CO;2.

Dunne, G.C., and Saleeby, J.B., 1993, Kern Plateau shear zone, southern Sierra Nevada—New data concerning age and northward continuation: Geological Society of America Abstracts with Programs, v. 25, no. 5, p. 89.

Dunne, G.C., and Suczek, C.A., 1991, Early Paleozoic eugeoclinal strata in the Kern Plateau pendant, southern Sierra Nevada, California, *in* Cooper, J.D., and Stevens, C.H., eds., Paleozoic Paleogeography of the Western United States, Volume 2: Los Angeles, Pacific Section, Society of Economic Paleontologists and Mineralogists Book 67, p. 677–692.

Gurnis, M., Hall, C., and Lavier, L., 2004, Evolving force balance during incipient subduction: Geochemistry Geophysics Geosystems, v. 5, no. 7, doi:10.1029/2003GC000681.

Hall, C.E., Gurnis, M., Sdrolias, M., Lavier, L.L., and Muller, R.D., 2003, Catastrophic initiation of subduction following forced convergence across fracture zones: Earth and Planetary Science Letters, v. 212, p. 15–30, doi:10.1016/S0012-821X(03)00242-5.

Hamilton, W., and Myers, W.B., 1966, Cenozoic tectonics of the western United States: Reviews of Geophysics, v. 4, p. 509–549, doi:10.1029/RG004i004p00509.

Haq, U.B., and Schutter, S.R., 2008, A chronology of sea-level changes: Science, v. 322, no. 5898, p. 64–68, doi:10.1126/science.1161648.

Holford, P.S., Green, P.F., Duddy, I.R., Turrer, J.P., Hills, R.R., and Stoker, M.S., 2009, Regional interplate exhumation episodes related to plate boundary deformation: Geological Society of America Bulletin, v. 121, no. 11/12, p. 1611–1628, doi:10.1130/B26481.1.

Ingersoll, R.V., Bullard, T.F., Ford, R.L., Grimm, J.P., Pickle, J.D., and Sares, S.W., 1984, The effect of grain size on detrital modes: A test of the Gazzi-Dickinson point-counting method: Journal of Sedimentary Petrology, v. 54, p. 103–116.

Ketner, K.B., 1986, Eureka quartzite in Mexico?—Tectonic implications: Geology, v. 14, p. 1027–1030.

Ketner, K.B., and Noll, J.H., 1987, Preliminary geologic map of the Cerro Cobachi area, Sonora, Mexico: U.S. Geological Survey Miscellaneous Field Studies Map, MF-1980, scale 1:20,000.

Kiehl, J.T., and Shields, C.A., 2005, Climate simulation of the latest Permian: Implications for mass extinction: Geology, v. 33, no. 9, p. 757–760, doi:10.1130/G21654.1.

Kistler, R.W., and Peterman, Z.E., 1973, Variations in Sr, Rb, K, Na, and initial $^{87}Sr/^{86}Sr$ in Mesozoic granitic rocks and intruded wall rocks in central California: Geological Society of America Bulletin, v. 84, p. 3489–3512, doi:10.1130/0016-7606(1973)84<3489:VISRKN>2.0.CO;2.

Marsaglia, K.M., 2012, Sedimentation at plate boundaries in transition, *in*, Busby, C., and Pérez, A., eds., Tectonics of Sedimentary Basins: Recent Advances: Chichester, UK, John Wiley & Sons, Ltd., doi: 10.1002/9781444347166.ch14.

Marsaglia, K.M., and Ingersoll, R.V., 1992, Compositional trends in arc-related, deep-marine sand and sandstone: A reassessment of magmatic-arc provenance: Geological Society of America Bulletin, v. 104, p. 1637–1649, doi:10.1130/0016-7606(1992)104<1637:CTIARD>2.3.CO;2.

Marsaglia, K.M., and Tazaki, K., 1992, Diagenetic trends in ODP Leg 126 sandstones, *in* Taylor, B., Fujioka, K., et al., eds., Proceedings of the Ocean Drilling Program, Scientific Results, Volume 126: College Station, Texas, Ocean Drilling Program, p. 125–138.

Martin, M.W., and Walker, J.D., 1995, Stratigraphy and paleogeographic significance of metamorphic rocks in the Shadow Mountains, western Mojave Desert, California: Geological Society of America Bulletin, v. 107, p. 354–366, doi:10.1130/0016-7606(1995)107<0354:SAPSOM>2.3.CO;2.

Miller, J.S., Glazner, A.F., Walker, J.D., and Martin, M.W., 1995, Geochronologic and isotopic evidence for Triassic–Jurassic emplacement of the eugeoclinal allochthon in the Mojave Desert region, California: Geological Society of America Bulletin, v. 107, p. 1441–1457, doi:10.1130/0016-7606(1995)107<1441:GAIEFT>2.3.CO;2.

Nichols, G., 1999, Sedimentology and Stratigraphy: Oxford, UK, Blackwell Science Ltd., 355 p.

Nikolaeva, K., Gerya, T.V., and Marques, F.O., 2011, Numerical analysis of subduction initiation risk along the Atlantic American passive margins: Geology, v. 39, p. 463–466, doi:10.1130/G31972.1.

Niu, Y., O'Hara, M.J., and Pearce, J.A., 2003, Initiation of subduction zones as a consequence of lateral compositional buoyancy contrast with the lithosphere: A petrological perspective: Journal of Petrology, v. 44, no. 5, p. 851–866, doi:10.1093/petrology/44.5.851.

Prothero, D.R., 1998, Bringing Fossils to Life: New York, McGraw-Hill, 457 p.

Rains, J.L., 2009, The Stratigraphic and Petrologic Record of Subduction Initiation in the Permian Metasedimentary Succession of the El Paso Mountains, Kern County, California [M.S. thesis]: Northridge, California, California State University, Northridge, 138 p.

Saleeby, J.B., 2011, Geochemical mapping of the Kings-Kaweah ophiolite belt, California—Evidence for progressive mélange formation in a large offset transform-subduction initiation environment, *in* Wakabayashi, J., and Dilek, Y., eds., Mélanges: Processes of Formation and Societal Significance: Geological Society of America Special Papers 480, p. 31–73.

Saleeby, J.B., and Busby-Spera, C., 1992, Early Mesozoic tectonic evolution of the western U.S. Cordillera, *in* Burchfiel, B.C., Lipman, P.W., and Zoback, M.L., eds., The Cordilleran Orogen: Boulder, Colorado, Geological Society of America, Geology of North America, v. G-3, p. 107–168.

Smith, G.A., and Landis, C., 1995, Intra-arc basins, *in* Busby, C.J., and Ingersoll, R.V., eds., Tectonics of Sedimentary Basins: Malden, Massachusetts, Blackwell Sciences, p. 263–298.

Snow, J.K., 1992, Large-magnitude Permian shortening and continental-margin tectonics in the southern Cordillera: Geological Society of America Bulletin, v. 104, p. 80–105, doi:10.1130/0016-7606(1992)104<0080:LMPSAC>2.3.CO;2.

Stern, R.J., 2004, Subduction initiation: Spontaneous and induced: Earth and Planetary Science Letters, v. 226, p. 275–292.

Stevens, C.H., and Stone, P., 2007, The Pennsylvanian–Early Permian Bird Spring Carbonate Shelf, Southeastern California: Fusulinid Biostratigraphy, Paleogeographic Evolution, and Tectonic Implications: Geological Society of America Special Paper 429, 82 p.

Stevens, C.H., Stone, P., Dunne, G.C., Greene, D.C., Walker, J.D., and Swanson, B.J., 1997, Paleozoic and Mesozoic evolution of east-central California: International Geology Review, v. 39, no. 9, p. 788–829, doi:10.1080/00206819709465303.

Stevens, C.H., Stone, P., and Miller, J.S., 2005, A new reconstruction of the Paleozoic continental margin of southwestern North America: Implications for the nature and timing of continental truncation and the possible role of the Mojave-Sonora megashear hypothesis, *in* Anderson, T.H., Nourse, J.A., McKee, J.W., and Steiner, M.B., eds., The Mojave-Sonora Megashear Hypothesis: Development, Assessment, and Alternatives: Geological Society of America Special Paper 393, p. 597–618.

Stewart, J.H., McMenamin, M.A.S., and Morales-Ramirez, J.M., 1984, Upper Proterozoic and Cambrian rocks in the Caborca region, Sonora, Mexico—Physical stratigraphy, biostratigraphy, paleocurrent studies, and regional relations: U.S. Geological Survey Professional Paper 1309, 36 p.

Stewart, J.H., Poole, F.G., Ketner, K.B., Madrid, R.J., Roldan-Quintana, J., and Amaya-Martinez, R., 1990, Tectonics and stratigraphy of the Paleozoic and Triassic southern margin of North America, Sonora, Mexico, *in* Gehrels, G.E., and Spenser, J.E., eds., Geological Excursions through the Sonora Desert Region, Arizona and Sonora: Arizona Geological Survey Special Paper 7, p. 182–202.

Stone, P., 1984, Stratigraphy, Depositional History, and Paleogeographic Significance of Pennsylvanian and Permian Rocks in the Owens Valley–Death Valley Region, California [Ph.D. thesis]: Stanford, California, Stanford University, 399 p.

Stone, P., and Stevens, C.H., 1984, Stratigraphy and depositional history of the Pennsylvanian and Permian rocks in the Owens valley–Death Valley region, eastern California, *in* Lintz, J., Jr., ed., Western Geological Excursions: Reno, Nevada, Department of Geological Sciences, McKay School of Mines, v. 4, p. 94–119.

Stone, P., Swanson, B.J., Stevens, C.H., Dunne, G.C., and Priest, S.S., 2009, Geologic Map of the Southern Inyo Mountains and Vicinity, Inyo County, California: U.S. Geological Survey Scientific Investigations Map 3094, 1:24,000.

Sutherland, R., Barnes, P., and Uruski, C., 2006, Miocene–Recent deformation, surface elevation, and volcanic intrusion of the overriding plate during subduction initiation, offshore southern Fiordland, Puysegur margin, southwest New Zealand: New Zealand Journal of Geology and Geophysics, v. 49, p. 131–149, doi:10.1080/00288306.2006.9515154.

Tabor, N.J., and Montañez, I.P., 2002, Shifts in late Paleozoic atmospheric circulation over western equatorial Pangea: Insights from pedogenic mineral $\delta^{18}O$ compositions: Geology, v. 30, no. 12, p. 1127–1130, doi:10.1130/0091-7613(2002)030<1127:SILPAC>2.0.CO;2.

Walker, J.D., 1988, Permian and Triassic rocks of the Mojave Desert and their implications for timing and mechanisms of continental truncation: Tectonics, v. 7, p. 685–709, doi:10.1029/TC007i003p00685.

Winguth, A.M.E., Heinze, C., Kutzbach, J.E., Maier-Reimer, E., Mikdajewicz, R.D., Rees, A., and Ziegler, A.M., 2002, Simulated warm polar currents during the middle Permian: Paleoceanography, v. 17, no. 4, p. 1057, doi:10.1029/2001PA000646.

Zahler, M.A., 2006, Evaluation of stratigraphic data-management and displays using GIS and HTML: Example from the Permian Western Interior, U.S.A.: www.cefns.nau.edu/~rcb7/ (accessed 28 December 2008).

MANUSCRIPT RECEIVED 7 JULY 2011
REVISED MANUSCRIPT RECEIVED 7 FEBRUARY 2012
MANUSCRIPT ACCEPTED 19 FEBRUARY 2012

Printed in the USA